UNIVERSITY OF TURKU

Chemically synthesized poly(3,4-ethylenedioxythiophene)–reduced graphene oxide nanocomposite for supercapacitor applications

Master's Thesis in Materials Chemistry

Department of Chemistry

Author:

Siyuan Peng

Supervisors:

Dr. Plawan Kumar Jha

Prof. Carita Kvarnström

16.05.2024

Turku

The originality of this thesis has been checked in accordance with the University of Turku quality assurance system using the Turnitin Originality Check service.

Master's thesis

Subject: Materials Chemistry
Author(s): Siyuan Peng
Title: Chemically synthesized poly(3,4-ethylenedioxythiophene)–reduced graphene oxide nanocomposite for supercapacitor applications
Supervisor(s): Dr. Plawan Kumar Jha, Prof. Carita Kvarnström
Number of pages: 46 pages
Date: 16.05.2024

Abstract

Supercapacitors have become popular as essential energy storage devices because of their remarkable energy density, outstanding power density, and exceptional stability cycles. The choice of electrode active material is a crucial factor in determining the superior electrochemical performance of supercapacitors. Poly(3,4-ethylenedioxythiophene) (PEDOT) has the advantage of excellent chemical stability, good cost-effectiveness, and an easy synthesis process to be used as the electrode active material. Nevertheless, it also suffers from drawbacks, such as short electrochemical stability cycles, low surface area, and low theoretical capacitance. To deal with these issues, reduced graphene oxide (RGO) is proposed due to its notable benefits, including its high specific surface area, excellent conductivity, high theoretical capacitance, and extended cycle stability. This thesis work involves the chemical synthesis of a PEDOT-RGO nanocomposite utilizing an in-situ oxidation-reduction approach. The performance of a symmetrical 2-electrode supercapacitor made from a nanocomposite of PEDOT-RGO was evaluated in 1 M H_2SO_4 electrolyte. The PEDOT-RGO has a maximum specific capacitance of 158 F/g when subjected to a current density of 0.25 A/g. Furthermore, it maintains over 80% of its capacitance after conducting 10000 continuous galvanic charge-discharge (GCD) cycles. Furthermore, the PEDOT-RGO supercapacitor demonstrated enhanced energy and power density, with approximately 1 Wh/kg and 351 W/kg increase, respectively, compared to PEDOT. These findings suggest that the incorporation of RGO into PEDOT improves its supercapacitive performance, offering the potential for developing high-performance supercapacitors.

Keywords: PEDOT, reduced graphene oxide, supercapacitor

Table of contents

1 Introduction 7

1.1 Supercapacitor 8

1.1.1 Electrical double layer capacitor 11

1.1.2 Pseudocapacitive supercapacitor 13

1.1.3 Applications of supercapacitor 13

1.2 Conducting polymer 15

1.3 Graphene 17

1.4 Electrode materials for supercapacitor 21

1.4.1 PEDOT 21

1.4.2 Reduced graphene oxide 23

1.5 Purpose and objective 25

2 Experimental section 27

2.1 Materials 27

2.2 Experimental equipment 27

2.3 Preparation of PEDOT-RGO 28

2.4 Preparation of PEDOT-RGO electrodes 30

2.5 Characterization of PEDOT-RGO nanocomposite 31

2.5.1 XRD 31

2.5.2 Raman spectroscopy 32

2.5.3 SEM 34

2.5.4 Electrochemical workstation 35

3 Results 39

3.1 Identification of PEDOT-RGO nanocomposites 39

3.2 Electrochemical characterization of PEDOT-RGO supercapacitors 40

4 Conclusion and discussion 46

References 47

Acknowledgment

Here, I would like to express my sincere gratitude to my supervisors Dr. Plawan Kumar Jha and Prof. Carita Kvarnström for their invaluable assistance throughout the entire experimental project. Dr. Plawan Kumar Jha's professional knowledge, rich operational experience, and guidance played a vital role in the smooth progress of this experimental project. Prof. Carita Kvarnström’s insightful feedback and encouragement also significantly contributed to my thesis work. I am deeply grateful for their dedication, patience, and guidance, which were crucial in helping me overcome various challenges during the project.

Abbreviations and terms

PEDOT	poly (3,4-ethylenedioxythiophene)
RGO	reduced graphene oxide
Fe(III)PTS	Iron(III) p-toluenesulfonate
GCD	galvanic charge-discharge
EDL	electric double layer
EDLC	electrical double layer capacitors
CPs	conducting polymers
LEDs	light-emitting diodes
OFETs	organic field-effect transistors
CVD	chemical vapor deposition
EDOT	3,4-Ethylenedioxythiophene
GO	graphene oxide
VPP	vapor phase polymerization
ESR	equivalent series resistance
NMP	N-Methyl-2-pyrrolidone
SEM	X-ray powder diffraction
SE	scanning electron microscope
BSE	secondary electrons
CV	backscattered electrons
EIS	electrochemical impedance spectroscopy

1 Introduction

The necessity for developing sustainable, environmentally friendly, and efficient systems for storing energy has grown more pressing as a result of fast industrialization and technological progress.[1,2] The over-dependence on fossil fuels and energy sources that are not renewable has led to a severe worldwide energy crisis. The discontinuous characteristics of energy from renewable sources provide difficulty in incorporating them into electrical networks, necessitating a harmonization between energy production and consumption.[3] This urgency is also emphasized by the increasing expenses of fuels, degradation of the environment, and geopolitical problems linked to reliance on fossil resources. In response to these issues, there is an increasing focus on developing storage systems with high power and energy density. These technologies have the goal of reducing the increasing global power demand and offering a sustainable and environmentally friendly substitute for conventional energy sources.[4-6]

Energy storage systems are crucial for mitigating the variability of energy generated from renewable energies as well as improving the amount of electricity delivered into the electrical system from sources like wind and solar power. Batteries, fuel cells, and supercapacitors play a significant role in various energy storage systems. Fuel cells and batteries both utilize redox processes at the electrodes to transform chemical energy into electrical energy. However, a key distinction is that fuel cells require a constant fuel source in order to operate efficiently. Batteries are characterized by a single compartment where storage and conversion of energy occurs, making them closed systems. In contrast, fuel cells are open systems where the compartments for storing and converting energy are divided.[4,5]

In order to enhance a vehicle's efficiency, the storage of kinetic energy when the vehicle decelerates or stops is essential. While traditional methods, batteries have been effectively used for low-power activities, achieving higher efficiency would need significant power, which can only be supplied by alternative forms of energy storage like supercapacitors. Supercapacitors utilize an electric double layer (EDL) at the interface of the electrode and electrolyte to absorb and release ions, enabling the storage and release of energy. These devices possess distinctive characteristics, such

as a high power density and fast charging/discharging speeds, extended duration, and safe operation. These attributes offer numerous advantages, such as shortened charging durations from hours to minutes, enhanced reliability of renewable electricity, waste reduction, and eco-friendly material utilization. Furthermore, supercapacitors excel in combining the energy density features of batteries with the power discharge properties of capacitors. Supercapacitors possess these properties, and so represent an innovative technology that bridges the gap between batteries and capacitors, resulting in a device that is both highly efficient and small.[1,5,7]

Figure 1 presents a Ragone plot that provides a comparative analysis of the energy and power densities of batteries, fuel cells, and supercapacitors.

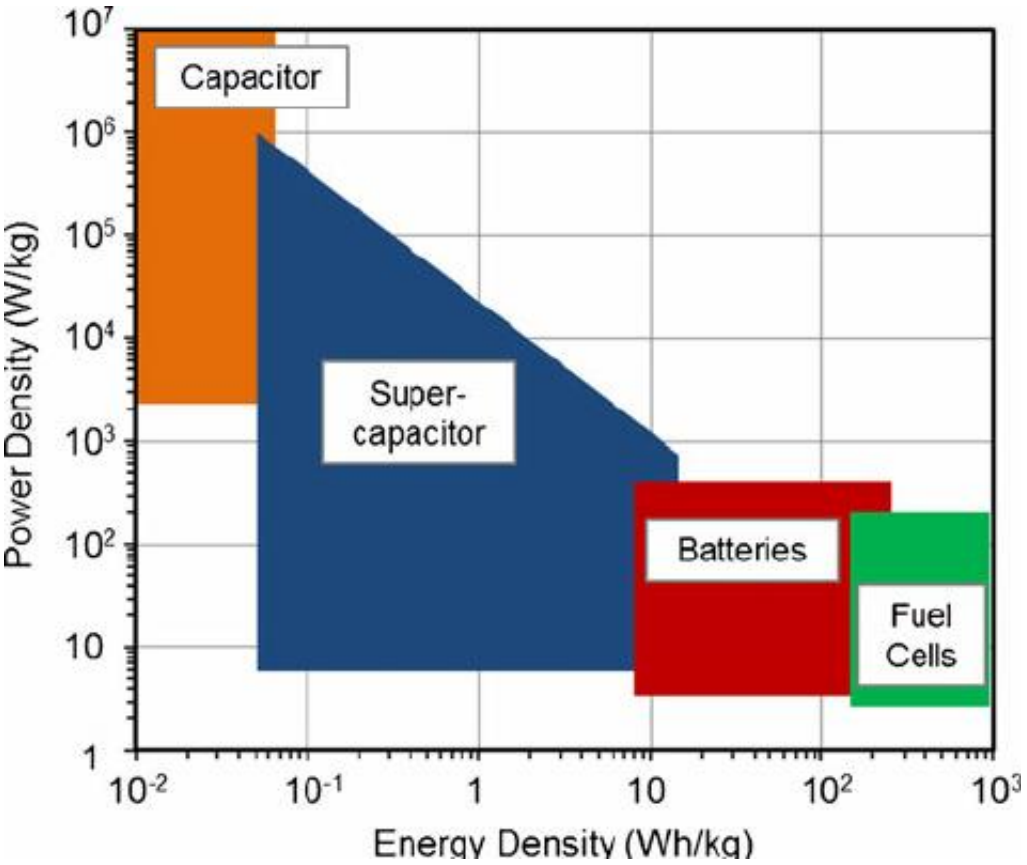

Figure 1. Ragone plot of various energy storage systems.[8]

1.1 Supercapacitor

Supercapacitors are devices for storing energy that possess a greater capacity and capacitance compared to conventional capacitors. They have gained significant

interest in the past few decades due to their exceptional performance in energy storage and release, as well as their extended lifespan. Supercapacitors differ from conventional rechargeable batteries in that they store energy by electrostatic methods, enabling them to rapidly discharge massive quantities of power. Furthermore, as compared to electrolytic capacitors, supercapacitors often possess a capacity to store 10 to 100 times more energy per unit volume or mass. The aforementioned benefits make supercapacitors ideal for applications that need frequent charge-discharge cycling.[9,10] Table 1 shows a comparison of the characteristics of supercapacitors, batteries, and capacitors.

Table 1. Comparative analysis of capacitors, supercapacitors, and batteries.[11]

Property	Capacitor	Supercapacitor	Battery
Energy density (Wh/kg)	<0.1	1–10	10–100
Power density (W/kg)	>>10,000	500–10,000	< 1000
Discharge time	10^{-6} to 10^{-3} s	s to min	0.3–3 h
Charge time	10^{-6} to 10^{-3} s	s to min	1–5 h
Coulombic efficiency (%)	~100	85–98	70–85
Cycle-life	Infinite	>500,000	~1000

Figure 2 displays the fundamental configuration of a supercapacitor, which normally has two conductive electrodes that are divided by an electrolyte and a separator that is used for transferring ionic charge and preventing internal short circuits. Additionally, each electrode is connected to a current collector to collect the charge from the active material and enable the transfer of current to external circuits. The features of supercapacitors are determined by the interaction of the materials contained within them. The performance and thermal and electrical characteristics of supercapacitors are influenced mainly through the use of electrode material and the specific electrolyte employed. The electrodes often need excellent conductivity, a high surface area

relative to volume and mass, high chemical stability, and the capacity to store a significant amount of charge. Aqueous and organic electrolytes are often employed in supercapacitors, selected for their conductivity and stability at high voltages. Supercapacitors that use aqueous electrolytes typically have an operating voltage limit of 1 V. However, supercapacitors that use organic electrolytes can operate at voltages of 2.7 V or more in order to achieve high specific energy. It is important to note that using organic electrolytes also results in higher specific resistance, which in turn reduces the specific power of the supercapacitor.[4] Applying a voltage to the electrode causes the ions in the electrolyte to create an electric double layer with a charge opposite to that of the electrode. This results in the formation of an electric field, allowing the capacitor to store energy.[10]

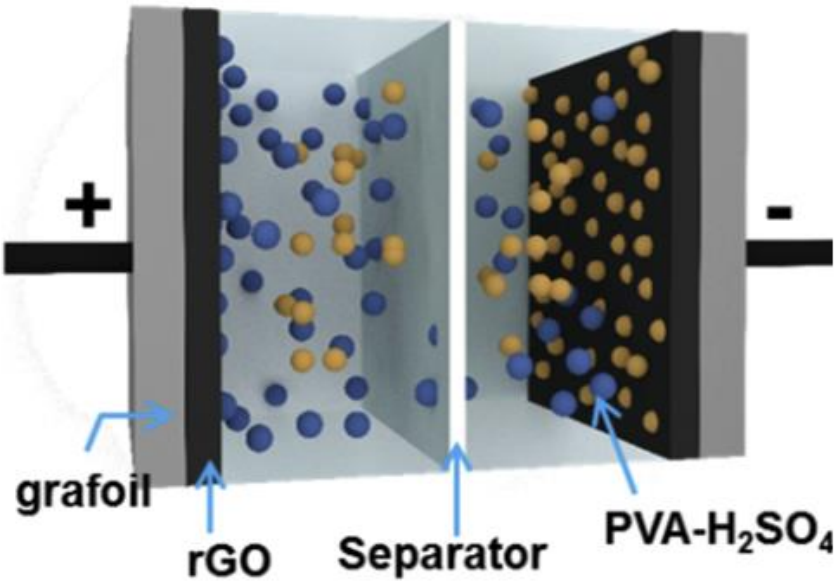

Figure 2. Schematic illustration of a RGO supercapacitor.[12]

According to the energy storage mechanisms and structures, supercapacitors are typically classified into two primary categories: electrical double layer capacitors (EDLC) and pseudocapacitors.[5,7,13] Figure 3 displays the different categorizations of supercapacitors.

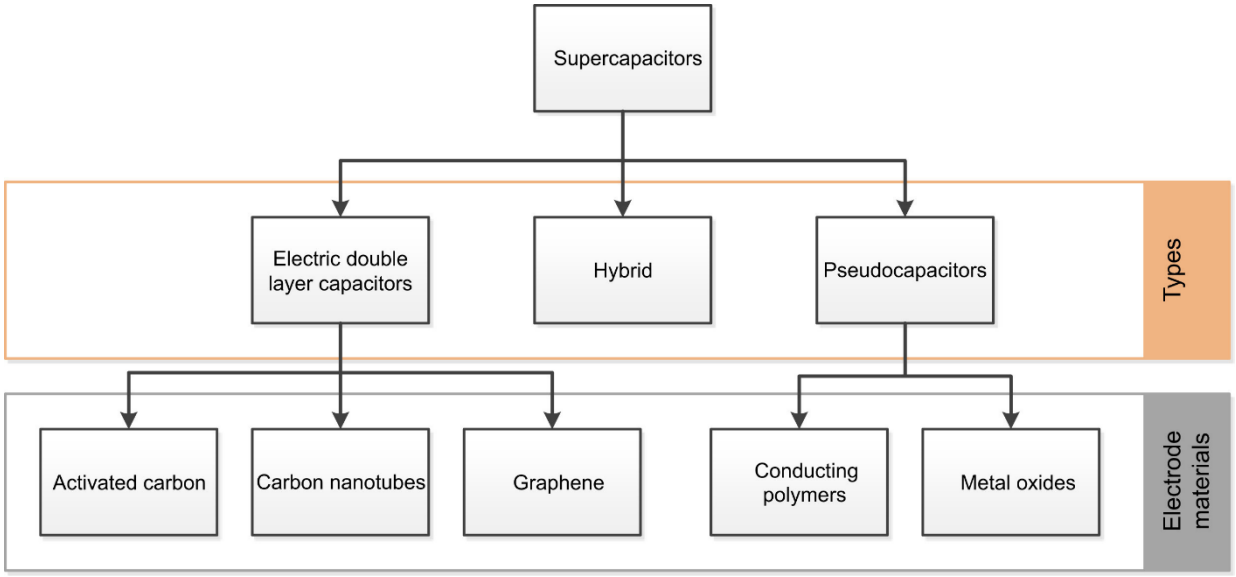

Figure 3. Different types of supercapacitors.[4]

1.1.1 Electrical double layer capacitor

Currently, EDLCs are the most recognized devices for storing energy that are extensively utilized in commercial applications. In 1957, H. I. Becker from General Electric Company was the first to present and obtain a patent for the concept of double-layer capacitance. In 1971, the Standard Oil Company of Ohio produced the initial commercial supercapacitor, which was subsequently utilized by the Japanese corporation NEC for memory applications.[7] EDLCs consist of two electrodes made of carbon, an electrolyte, and a separator. Figure 4 presents a diagram illustrating an EDLC. Similar to traditional capacitors, EDLCs store charge through electrostatic methods without any transfer of charge at the contact between the electrode and electrolyte.[10]

The formation of a double layer is used to prevent the recombination of ions in electrodes. EDLCs achieve high energy density by utilizing the double layer, which is made possible by increasing the area of the surface and reducing the distance between electrodes.[13] Since non-Faradaic processes do not involve any transmission of charge in the electrolyte and electrode, resulting in no chemical or compositional modifications associated with them. Due to this factor, the ability of EDLCs to store charge is remarkably reversible, enabling them to attain exceptional cycle stabilities. EDLCs often exhibit consistent performance characteristics across a large number of charge-

discharge cycles, often reaching up to 10^6 cycles. However, electrochemical batteries typically have a maximum lifespan of around 10^3 cycles. EDLCs are highly suitable for use in non-user serviced regions, such as deep sea or mountain settings, due to their excellent cycle stability.[10]

Currently, the primary focus of research on EDLCs is to enhance the usage effectiveness of energy and their thermal stability. Carbon-based substances are plentiful and environmentally acceptable, possessing a large specific surface area, excellent conductive properties, great durability in chemicals, and a broad range of working temperatures. These materials show great potential as electrodes for supercapacitors. Carbon materials of different varieties are now extensively utilized as electrode materials in commercially available EDLCs since they possess a highly effective specific surface area, an ideal volume of pore space and a well-balanced range of pore diameters, as well as outstanding electrical conductivity.[7]

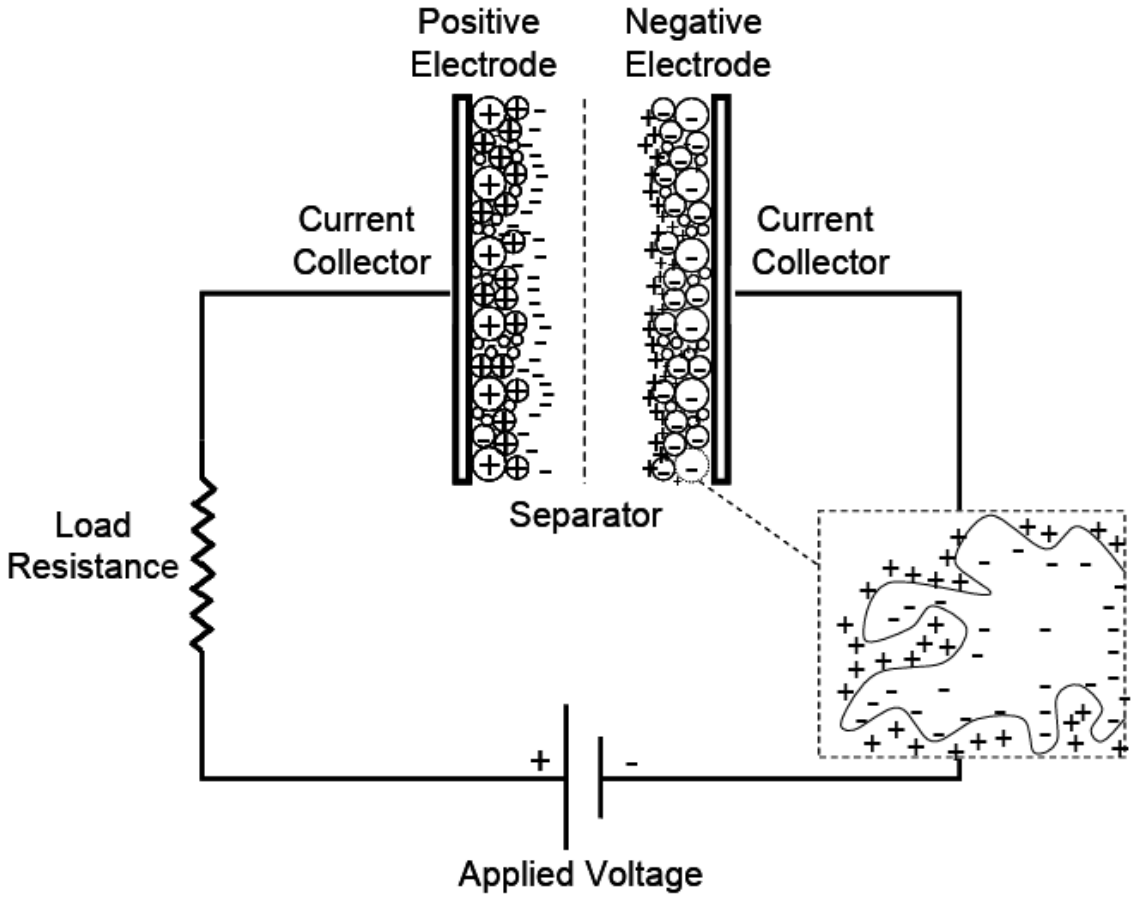

Figure 4. Schematic illustration of an EDLC.[10]

1.1.2 Pseudocapacitive supercapacitor

Conway introduced the Faraday quasi-capacitor mechanism in 1951, which proposed a process in which charging potential of the electrode occurs by underpotential deposition, including reversible redox processes of adsorption and desorption. The charge storage process in such capacitor involves the accumulation of charge on the double layer as well as the reactive processes that take place between the ions in the electrolyte and the electrode. When the applied electric field causes the charged particles in the electrolyte to move to the interface between the electrode and solution, they undergo redox reactions at the interface. This process leads to the accumulation of a substantial quantity of charge on the surface of the electrode. The reverse process of the redox reaction at the discharge step will send the ions that enter the oxide back to the electrolyte.[7] Figure 5 shows the basic configuration of a pseudocapacitor，which can achieve higher capacitance values and energy densities compared to EDLCs due to the Faradaic processes. Two common types of electrode materials for charge storage in pseudocapacitors are conductive polymers and metallic oxides.[10]

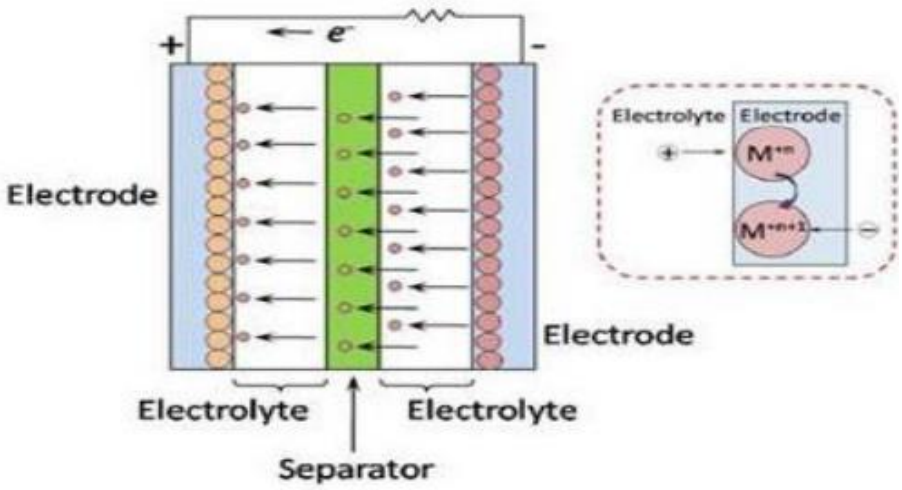

Figure 5. Schematic illustration of a pseudocapacitor.[13]

1.1.3 Applications of supercapacitor

Supercapacitors have numerous possible applications across different fields. For applications that need a high power density, frequent charge/discharge cycles, or a more extended life cycle stability, supercapacitors provide various benefits. For

example, supercapacitors can be employed in consumer electronics to provide short-term power backup and stabilize voltage levels. Furthermore, due to their better qualities compared to lead-acid batteries, supercapacitors are being increasingly used in UPS systems, electric automobiles, and various power-related applications. Recently, supercapacitors have been employed as an energy storage solution to enhance voltage stability in sustainable energy storage devices, hence regulating the power source and grid. Supercapacitors have the ability to provide a consistent power supply in situations when there are varying demands. Moreover, supercapacitors are essential components in many automotive applications since they possess the ability to store and release energy at a high rate efficiently. Some of these mentioned examples can be seen in Figure 6.[7,14]

Figure 6. Application examples of supercapacitors.[14]

1.2 Conducting polymer

Conducting polymers (CPs) are a type of substances that combines the characteristics of organic polymers with the conductive features of metals. Their unique conjugated structure enhances the mobility of charge carriers throughout the polymer chain, distinguishing them from traditional insulating polymers. And they have attracted considerable interest because of their distinctive electrical, optical, and mechanical characteristics.[15] CPs exhibit a high electrical conductivity compared to other materials. Figure 7 shows the difference in electrical conductive properties between conducting polymers alongside different substances. The conductivity in such polymers is attributed to two reasons: the presence of conjugated double bonds in the polymer chains and the phenomenon of doping. The presence of conjugated π electrons, together with dopant, enables the movement of electrons in CPs as carriers of charge. This causes the electrons to spread out and become delocalized in the conduction band, hence enhancing the polymer's metallic properties.[16]

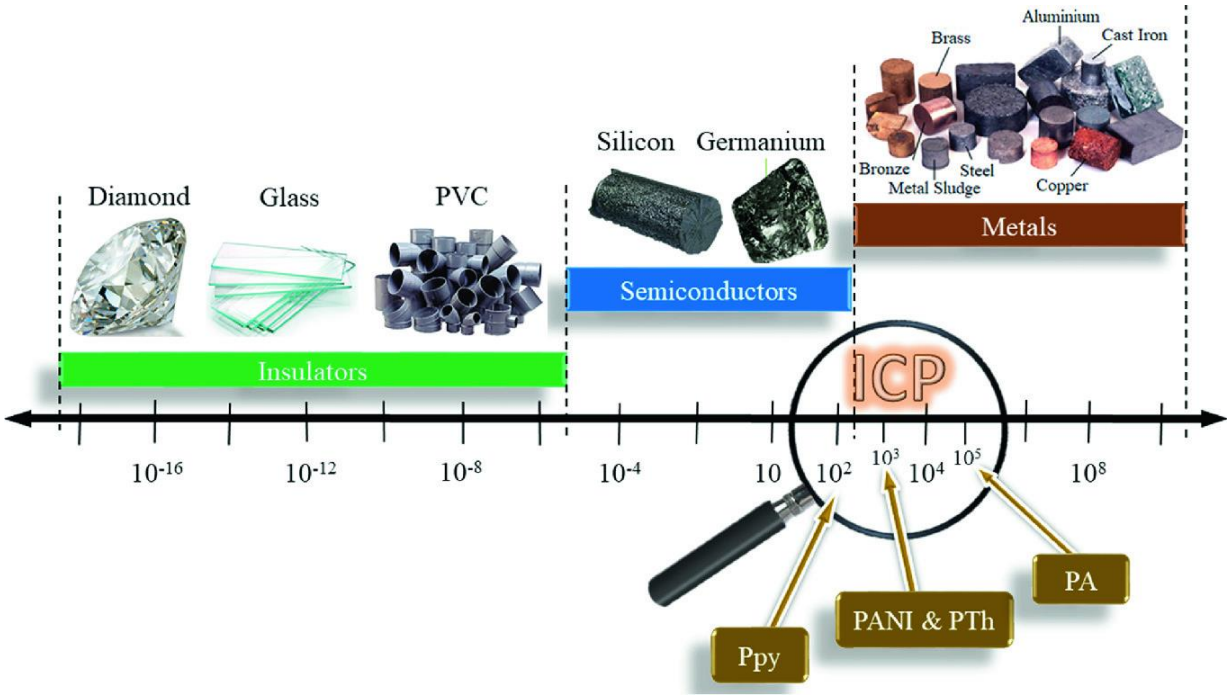

Figure 7. An evaluation of the conductivity of CPs in relation to other materials.[16]

CPs can typically undergo doping using two well-known methods: n-doping, which involves the addition of electrons, or p-doping, which involves the reduction of electrons. This can be achieved by introducing a different kind of dopant, as seen in

Figure 8.[16] Through the utilization of a redox reaction, the polymers undergo a transformation into electrically conductive by generating delocalized charge carriers. In order to achieve conductivity, the backbone of CPs needs to undergo oxidation or reduction to introduce charge centers.[15]

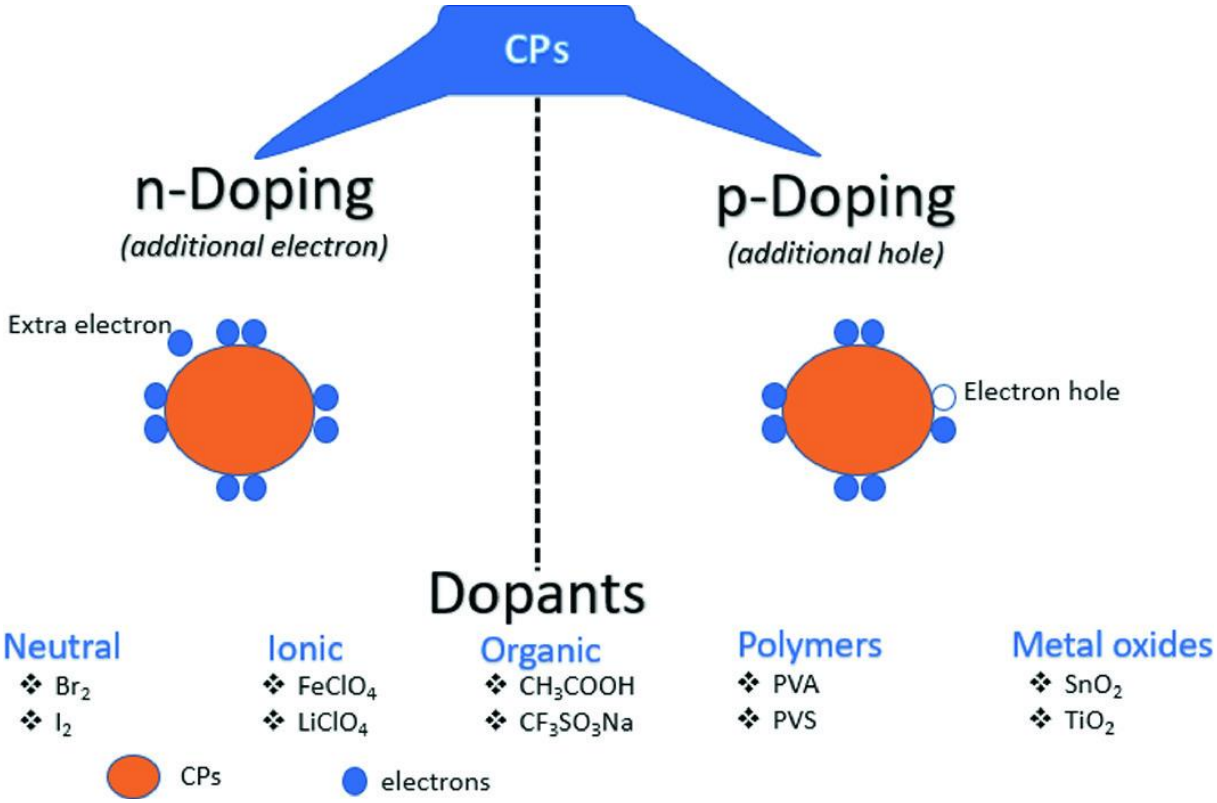

Figure 8. Classification of dopants used in CPs.[16]

CPs are very versatile across various fields because of their capacity to alter electrical conductivity, regulate chemical and electrochemical characteristics, affordable price, flexibility, chemical stability, simple synthesis, and excellent biocompatibility. Figure 9 illustrates the diverse applications of CPs. For example, CPs can be used as essential components in devices such as organic solar cells, light-emitting diodes (LEDs), and organic field-effect transistors (OFETs) due to their flexibility, lightweight nature, and compatibility with low-cost manufacturing processes. Besides, CPs have exceptional sensitivity to external stimuli in the field of sensing and detection, making them well-suited for chemical, biological, and gas sensors. In addition, when used as active materials for electrodes in the storage of energy devices, CPs can provide a significant capacity for storing charges, fast charging and discharging rates, and improved cycling stability. Moreover, within the field of biomedical engineering and

healthcare, CPs can be utilized as medication delivery methods as well as tissue engineering scaffolds, biosensors, and neural interfaces. This is possible due to their biocompatibility, adjustable mechanical characteristics, and capacity to interact with biological systems.[15,17,18]

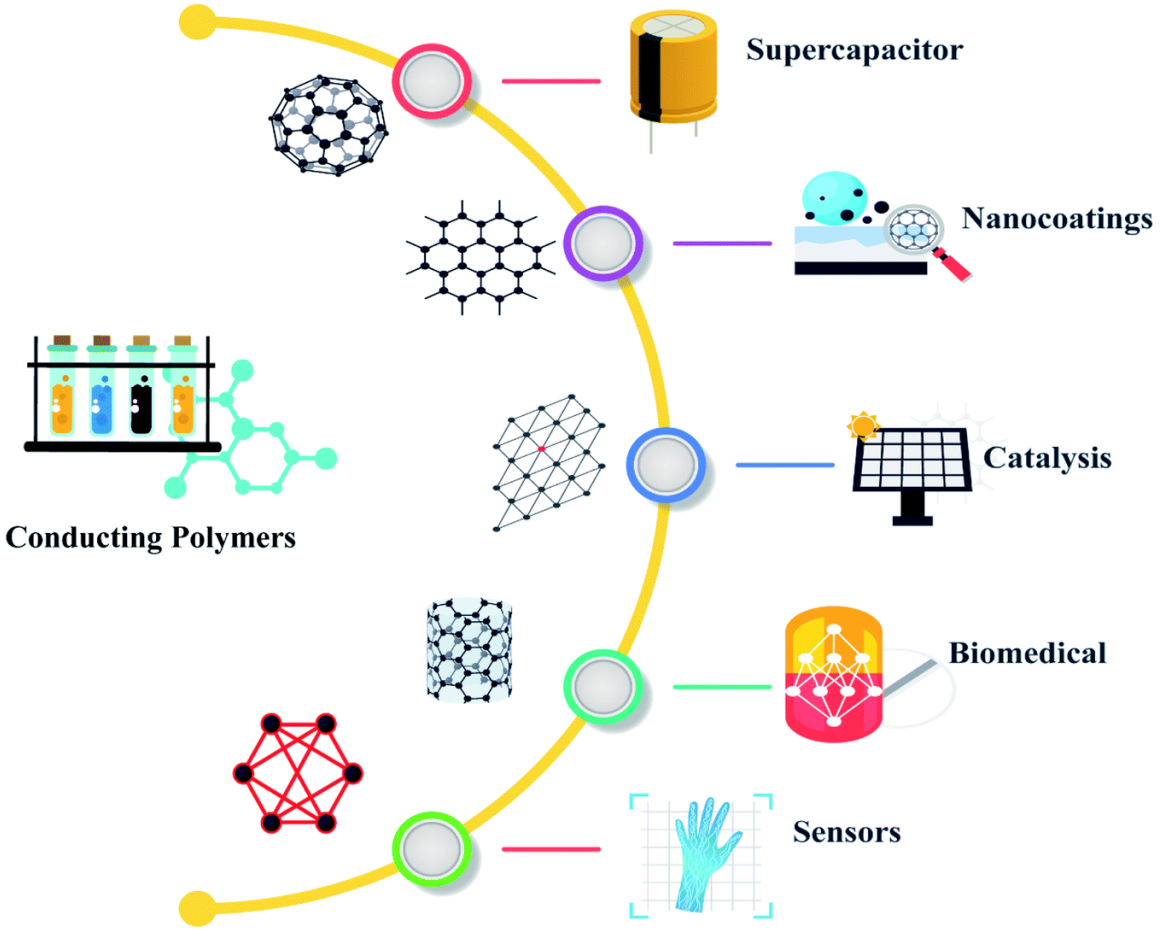

Figure 9. Applications of CPs.[19]

1.3 Graphene

Graphene is a breakthrough material that has attracted significant interest in the scientific and industrial fields since it was first isolated in 2004. Graphene has exceptional physical features and the capacity to adjust its chemical characteristics, which has led to a wide range of potential applications in various industries. Besides, graphene is also crucial for assessing the electronic characteristics of carbon allotropes and can be characterized by a honeycomb structure composed of hexagons.[20,21]

Graphene is a planar arrangement of atoms of carbon which are bonded together in a two-dimensional structure, with each carbon atom forming three covalent bonds in a sp^2 hybridization, and it consists of a monolayer hybrid nanosheet made up of sp^2 carbon atoms or several layers of carbon atoms. The carbon atoms in benzene rings are tightly packed and have had their hydrogen atoms removed.[21,22] Graphite is composed of many layers of graphene arranged in a stacked formation, with a distance of 3.35 Å between each layer. It is worth noting that a 1-mm-thick graphite crystal has around three million graphene monolayers. Graphene is categorized based on its electronic characteristics and is typically referred to as 'monolayer', 'bilayer', or 'few-layer' graphene (usually consisting of less than ten layers).[20] The honeycomb network of graphene serves as the fundamental unit for many major allotropes. Figure 10 shows some examples of the carbon allotropes. Graphene can either be arranged in a three-dimensional structure to create graphite, rolled into one-dimensional nanotubes, or wrapped to produce zero-dimensional fullerenes.[21]

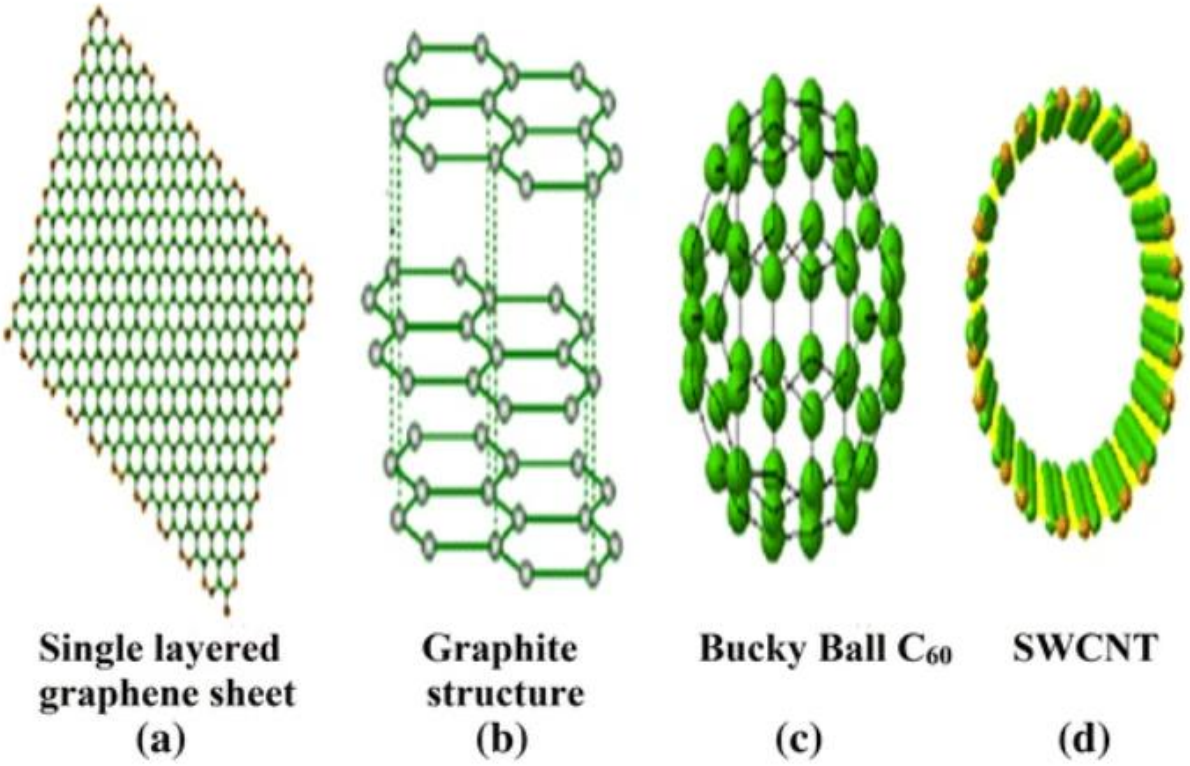

Figure 10. Schematic illustration of (a) Monolayer graphene. (b) Structure of graphite. (c) Fullerene. (d) Single-walled carbon nanotubes.[22]

Graphene is only a 2D and extremely thin substance; it has remarkable thermal, mechanical, and electrical features because of its extensive π-conjugation across long distances. This material's exceptional electrical conductivity, transparency, and flexibility have sparked the creation of numerous cutting-edge devices, including transistors, transparent conductive films, energy storage devices, drug delivery carriers, and sensors. Moreover, graphene's exceptional electrical characteristics make it a very attractive material for applications as transparent conducting electrodes.[20,21]

The manufacturing of graphene involves a diverse range of methodologies, such as mechanical exfoliation, chemical vapor deposition (CVD), epitaxial growth on silicon carbide, and reduction of graphene oxide, each with its own benefits and limits with regard to mass scale, quality, and objectives. A pioneering technique for synthesizing graphene is mechanical exfoliation, sometimes referred to as the "Scotch tape method." This approach includes the repetitive peeling of graphene layers from a bulk graphite source using adhesive tape. Although this process produces graphene of superior quality with outstanding electrical characteristics, its yield is restricted, and it requires a significant amount of labour, which makes it only appropriate for research uses. CVD is a highly popular method for producing graphene on a big scale. CVD is a process in which a carbon-containing gas, such as methane or ethylene, is broken down over a metallic catalyst substrate, typically copper or nickel, in an elevated environment. Carbon atoms undergo reassembly on the catalyst surface, resulting in the formation of a graphene layer. This layer can then be transferred to different substrates for further uses. CVD provides precise control over the thickness, quality, and ability to scale up graphene production, making it highly suitable for commercial uses such as electronics, energy storage, and material industry. Epitaxial growth on silicon carbide (SiC) substrates is another interesting technique for synthesizing graphene. In this method, graphene is formed spontaneously on the surface of SiC when heated in a controlled environment. This technique yields graphene of high quality with minimum imperfections, hence presenting promising possibilities for utilization in the fields of electronics and photonics. However, the advancement of epitaxial growth on SiC is limited by the lack of huge substrates and the complex nature of the synthesis process. The commonly used synthesis techniques of graphene, as well as its advantages and limitations, are illustrated in Figure 11.[23,24]

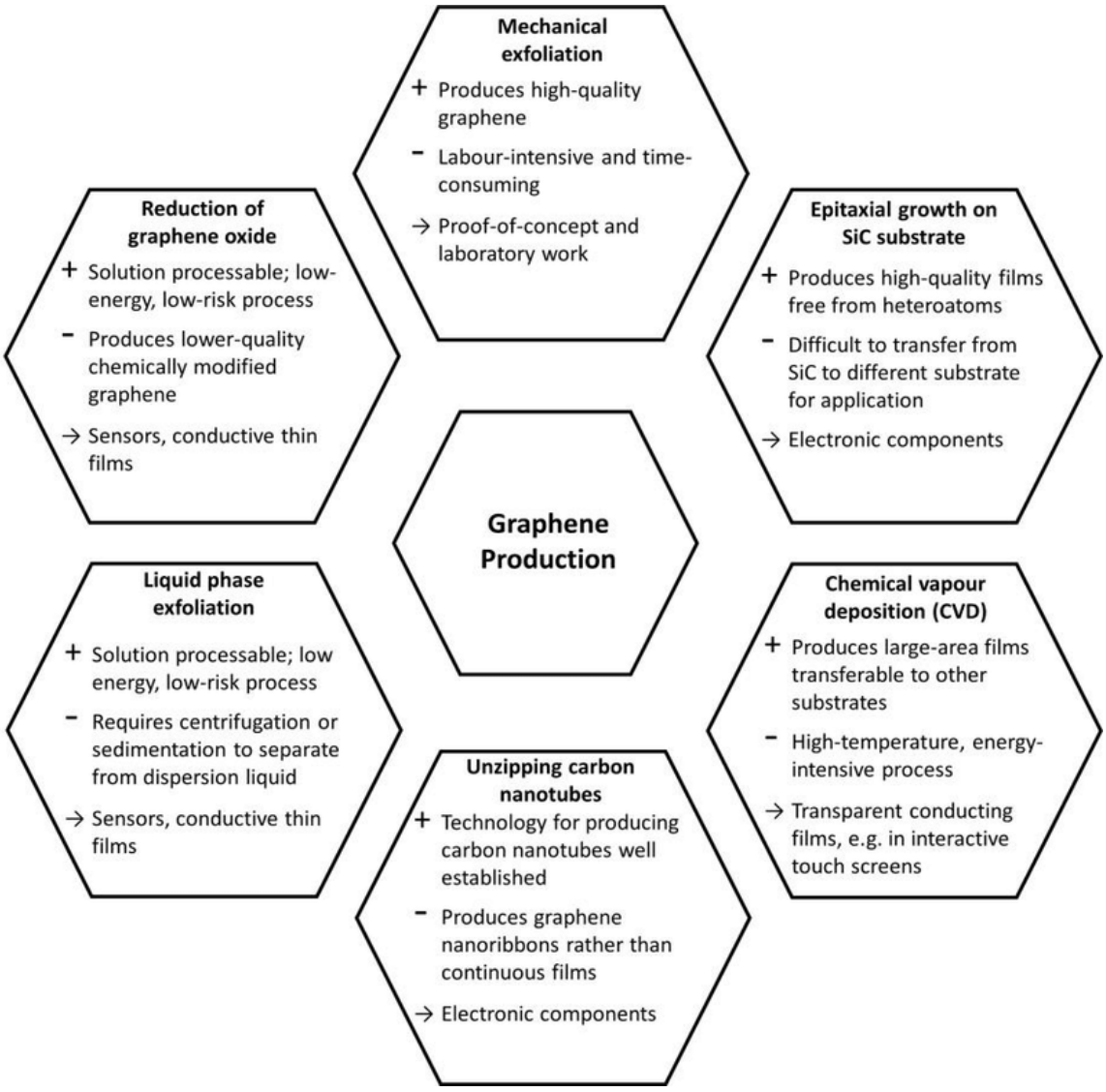

Figure 11. Common synthesis techniques of graphene.[24]

The outstanding characteristics of graphene have resulted in numerous applications in various industries. Table 2 shows various uses of graphene and its variants depending on their resistance. For example, Graphene's excellent conductive properties and large surface area have made it well-suited for using in batteries and supercapacitors. Graphene-based materials are utilized as electrodes to enhance their energy storage capacity, charge/discharge rates, and cycle stability. Moreover, it can also be used as a sensor. A monolayer sheet of graphene exhibits the capacity to detect a wide range of gasses and biomolecules. The sensing capability of the device relies on its expansive surface area and the alteration in conductance caused by surface adsorption. When molecules adhere to the surface of graphene, there is a charge transfer between the molecules and the graphene sheet, where the graphene can act

as either a donor or an acceptor. Chemical sensing in graphene is facilitated by variations in electrical resistance as well as carrier density.[22-25]

Table 2. Applications of graphene, according to their resistance.[22]

No.	Resistance range (Ω cm^2)	Applications
1	550–450	Touch screen
2	450–350	Smart electronic window
3	350–220	Flexible liquid crystal device
4	220–30	Flexible organic light-emitting diode
5	0.5–30	Solar cell

1.4 Electrode materials for supercapacitor

1.4.1 PEDOT

Poly(3,4-ethylenedioxythiophene), also known as PEDOT, is a highly versatile conductive polymer that has attracted considerable interest in both academic research and industry applications. Compared to other polythiophene derivatives, PEDOT has various favourable characteristics, which include a low oxidative potential and relatively small bandgap while maintaining excellent stability in the oxidized state.[26] PEDOT is a member of the conjugated polymer family, which can be identified by the presence of single bonds that alternate with double bonds throughout the backbone of the polymer. The unique arrangement of thiophene rings connected by ethylenedioxy linkers in PEDOT allows for the efficient spread of π-electrons, resulting in high electrical conductivity.[27] The molecular structure diagram of PEDOT is shown in Figure 12.

PEDOT can be synthesized with various methods. One method of synthesizing it is using chemical polymerization procedures, where the EDOT monomers are polymerized in the presence of oxidizing agents like Iron(III) chloride and ammonium persulfate. It can also be produced through an electrochemical polymerization process, which typically involves the use of three electrode setups: a counter electrode, a reference electrode, a working electrode, and a highly conductive substrate for achieving high crystallinity in PEDOT. Throughout the procedure, PEDOT polymers accumulate on the surface of the working electrode.[27]

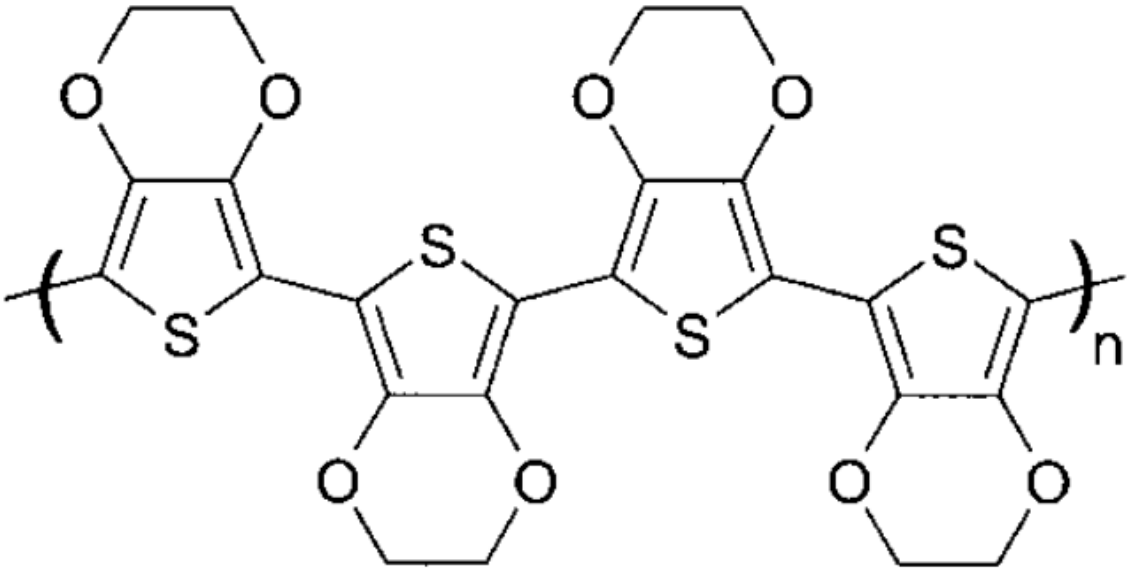

Figure 12. Molecular structure of PEDOT.[28]

Vapor phase polymerization (VPP) is another method for synthesizing PEDOT, where a film of the oxidizing agent combined with pyridine is exposed to EDOT vapors to commence the process of polymerization. The VPP offers a benefit over chemical synthesis, employing a bottom-up method, where the monomers are systematically arranged to form a highly organized crystalline structure.[29]

PEDOT has a diverse set of advantageous characteristics that enable it appropriate for a variety of applications, as seen in Figure 13. When PEDOT is made as a thin film, it has a high level of transparency, which makes it suitable for utilization as anti-static coatings for photographic films or as the active materials of the electrodes in supercapacitors.[26] The conductivity of PEDOT can be modulated by various stimuli, enabling precise identification of analytical substances. For biomedical applications, the biocompatibility, conductivity, and tunable characteristics of PEDOT render it a very appealing substance for interfacing with biological systems.[29]

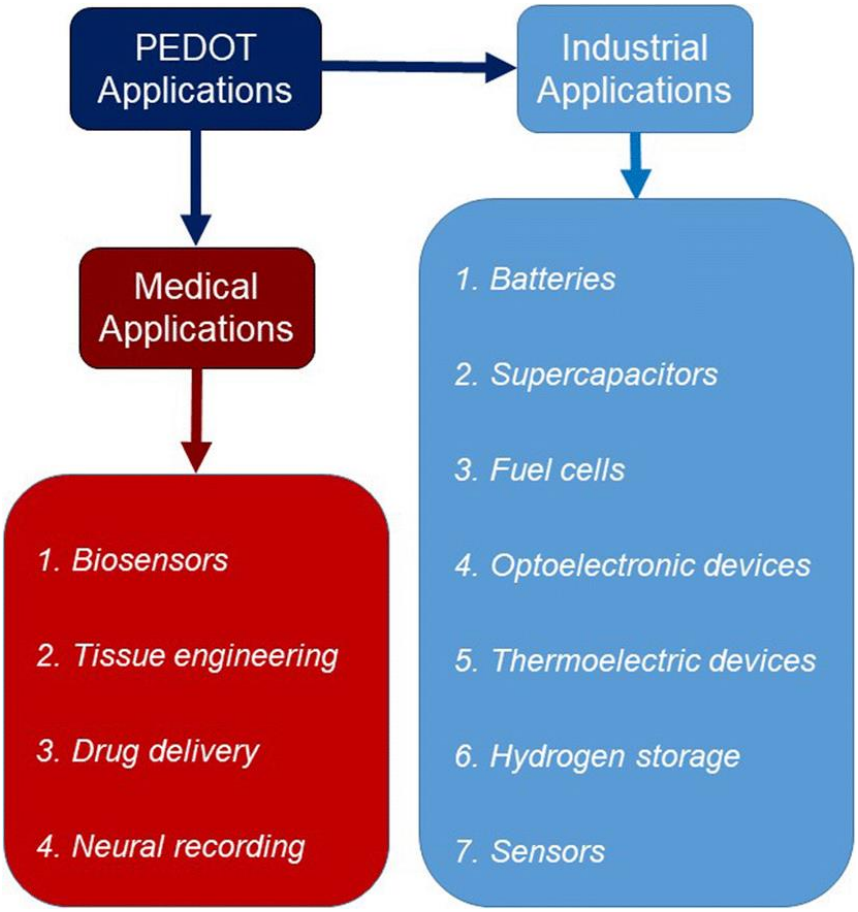

Figure 13. Various applications of PEDOT-based composites.[27]

1.4.2 Reduced graphene oxide

Reduced graphene oxide (RGO) is a versatile material with exceptional features, offering a bridge between the pristine graphene and its precursor, graphene oxide (GO). It is obtained by reducing GO, which is formed by oxidizing and exfoliating graphite. Through the reduction process, functional groups that contain oxygen, such as epoxides, hydroxyls, and carboxyls, are eliminated from the graphene oxide sheets, which leads to the restoration of the sp^2 carbon network and a partial recovery of characteristics similar to graphene. RGO exhibits comparable mechanical, optoelectronic, and conductive characteristics to pristine graphene due to its heterogeneous structure, which consists of a graphene-like basal plane adorned with structural defects and regions with oxygen groups. RGO possesses features similar to graphene, making it an extremely desired material for a wide range of applications, including sensors, biological and environmental applications, catalysis, and storage systems.[30]

Although graphene can be produced via a range of top-down techniques, such as mechanical exfoliation or bottom-up approaches like CVD, there is still a significant obstacle to the mass production of inexpensive, top-notch graphene. This limitation arises from the fact that some of the top-down methods can only be applied to stabilize graphene in liquid mediums. On the other hand, bottom-up methods need costly devices, involve synthesis at elevated temperatures, and are only applicable to particular metallic substrates that support the growth of high-quality graphene.[30]

On the contrary, when an enormous amount of graphene is needed for industrial applications, RGO is the most suitable option due to its ability to produce significant amounts of graphene with sufficient quality standards. GO possesses two significant features: firstly, it can be synthesized using low-cost graphite as the primary material and cost-effective chemical techniques, resulting in a high production yield. Secondly, GO exhibits a strong affinity for water and can form stable colloidal solutions, enabling the easy and inexpensive assembly of large-scale structures through simple solution-based methods.[30,31]

Various reduction processes, including chemical reduction, thermal reduction, hydrothermal reduction, and electrochemical reduction, can be used to synthesize RGO. These approaches provide the ability to control the degree of reduction, structure, and characteristics of the synthesized RGO, allowing customized designs for specific purposes. Figure 14 illustrates the transformation of GO into RGO by the elimination of oxygen functional groups. Chemical reduction is a cost-effective and straightforward technique that can be carried out at ambient temperature or with moderate heating. Typically, this approach depends on the utilization of chemical substances like hydrazine and ascorbic acid.[20,31] For thermal reduction methods it relies on quick annealing at elevated temperatures, which causes the separation of GO by expanding carbon monoxide or carbon dioxide gases produced by the breakdown of oxygen functional groups.[30]

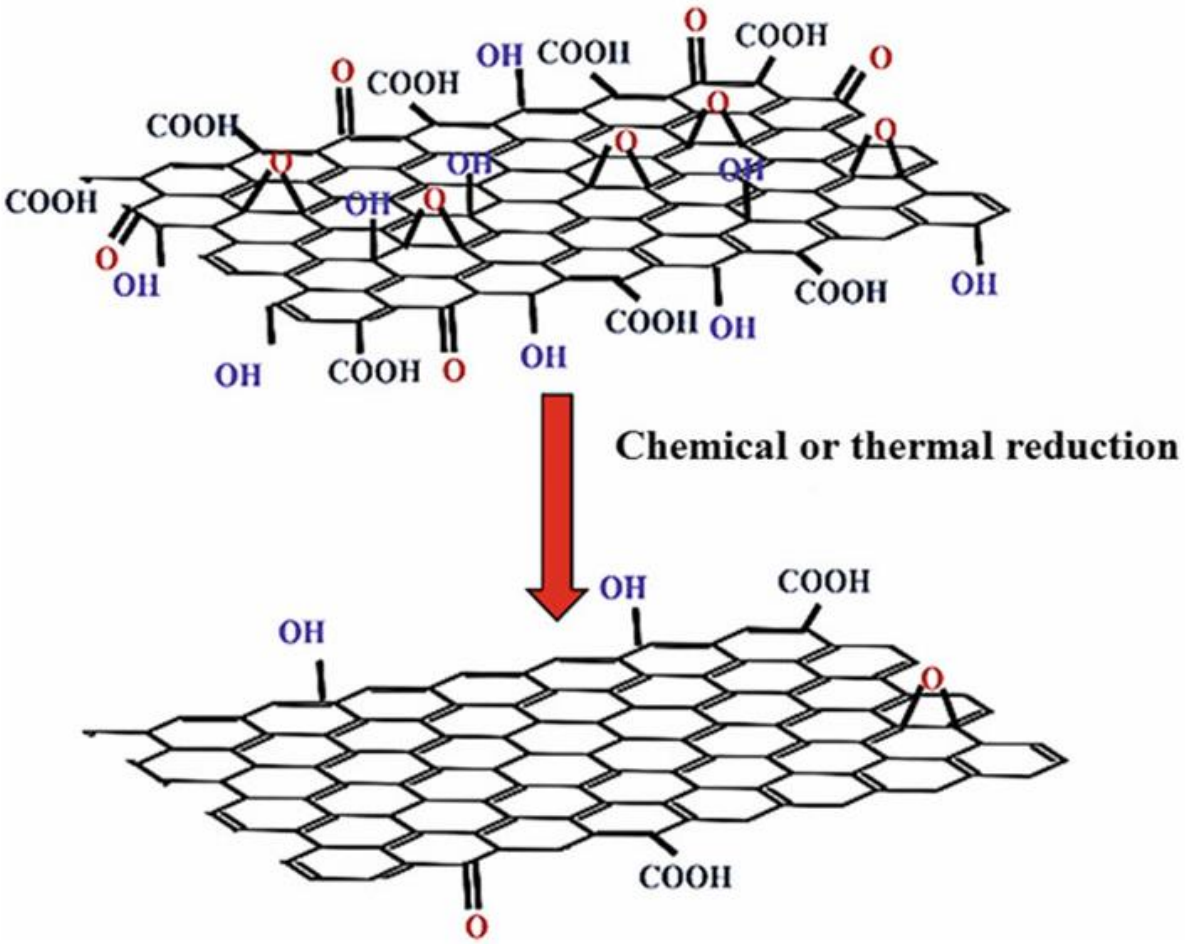

Figure 14. Schematic diagram of GO to RGO.[20]

1.5 Purpose and objective

The use of electrode active materials in supercapacitors plays a crucial role in determining the electrochemical performance of supercapacitors, and one of the desirable materials for the electrodes is conducting polymer. PEDOT offers benefits such as easy synthesis, processability, low cost, high conductivity, long-term environmental stability, and biocompatibility, making it one of the most popular candidates among conducting polymers. Besides, PEDOT has a relatively low equivalent series resistance (ESR), which causes an efficient charge transfer at the electrode-electrolyte interface and results in high power and energy density. Furthermore, PEDOT has excellent chemical stability, which is minimally affected by electrolytes and environmental conditions compared to other materials.

However, it also has drawbacks; for example, it does not have high theoretical capacitance, surface area, and long-life cycle stability. On the other hand, graphene possesses a high surface area, superior conductivity, high theoretical capacitance, and long-life stability, which makes it suitable for usage as a filler to enhance the supercapacitive performance of PEDOT. Therefore, the combination of PEDOT and graphene can be a promising candidate for high-performance supercapacitors.

This thesis work aims to modify PEDOT (synthesis of PEDOT-RGO nanocomposite via an in-situ oxidation-reduction method) to solve its problems of relatively small specific capacitance, relatively low specific surface area, and poor cycle stability, and the porous PEDOT-RGO nanocomposite was evaluated for performance in supercapacitor applications using a symmetric 2-electrode configuration.

2 Experimental section

2.1 Materials

Table 3 illustrates the experiment chemicals that were utilized during the experiment.

Table 3. Table of main experimental materials.

Name of the material	Manufacturer
3,4-Ethylenedioxythiophene (EDOT, > 98 %)	TCI
Graphene Oxide (GO)	Plawan Kumar Jha (UTU)
Iron(III) p-toluenesulfonate hexahydrate (Fe(III)PTS)	Sigma-Aldrich
Nafion (5%)	Sigma-Aldrich
N-Methyl-2-pyrrolidone (NMP, 99.5%)	TCI
Sulfuric acid (H_2SO_4, 1 mol/L)	Merck
Conductive carbon black	Nanografi
Graphite sheet (99.88% purity)	Thermo Scientific

2.2 Experimental equipment

Table 4 shows the main devices and analytical equipment together with their corresponding models utilized in this thesis work.

Table 4. Table of main experimental instruments.

Instrument	Model	Manufacturer
Centrifuge	Biofuge stratos	Heraeus
Ultrasonic cleaner	USC-THD	Avantor
Hot plate stirrer	MR Hei-Tec	Heidolph
Laboratory pellet press	GS15011	Specac
Scanning electron microscope		Bruker
Vacuum oven		Memmert
Raman microscope	RE 04	InVia
X-ray powder diffraction	Aeris	PANalytical
Potentiostat	A25352	Ivium

2.3 Preparation of PEDOT-RGO

The production involves the chemical synthesis of the PEDOT-RGO nanocomposite through an in-situ oxidation-reduction method. Figure 15 shows the synthesis process of PEDOT-RGO. In this process, Fe(III) acts as an oxidizing agent, transforming EDOT into PEDOT and being transformed into Fe(II) ions. Subsequently, these Fe(II) ions are used to chemically reduce graphene oxide. The following are the specific synthesis steps:

(1) A 5 mg/mL solution of GO was prepared by dissolving 250 mg of GO in 50 mL of distilled water using sonication for a duration of 2 hours.

(2) Approximately 4.12 gm of Fe(III)PTS and 25 mL of de-ionized water were put together in a 100 mL round bottom flask. The mixture was then subjected to sonication and stirring at a temperature of 94 degrees Celsius for a duration of 15 minutes.

(3) Following a duration of 15 minutes, a volume of 0.688 mL of EDOT was gradually added into the mixture and then stirred at a temperature of 94 ^{o}C for another 15 minutes.

(4) After an interval of 15 minutes, a volume of 10 mL of GO solution with a concentration of about 5 mg/mL was added to the previously mentioned mixture., which was then reacted for 24 hours under stirring and heating at 94 ^{o}C.

(5) When the mixture reached ambient temperature via natural cooling, it was subjected to centrifugation. The remained solid product was subsequently mixed thoroughly with distilled water and then subjected to centrifugation at 3500 RCF. The aforementioned steps were replicated three times, with a duration of five minutes for each repetition. Subsequently, ethanol was added to the product, which was thoroughly blended and subjected to centrifugation at a speed of 3500 RCF for a duration of 5 minutes. The aforementioned steps were repeated three times.

(6) The sample product was then vacuum dried at 40 ºC for 12 hours in a vacuum oven.

(7) The purified sample was exposed to a setting of 175 ºC for a period of 24 hours before further measurement.

Picture 1 displays the PEDOT-RGO nanocomposite that has been synthesized.

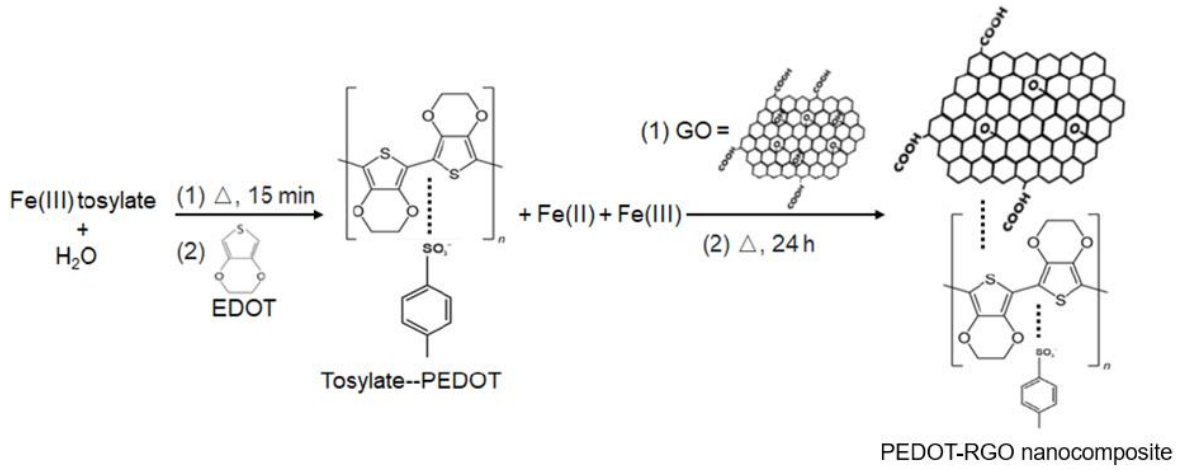

Figure 15. Diagrammatic representation of the PEDOT-RGO synthesis route.

Picture 1. PEDOT-RGO nanocomposite.

2.4 Preparation of PEDOT-RGO electrodes

(1) The substrate utilized was a graphite sheet, which was cut to dimensions of 4 x 5 cm.

(2) A mixture containing 6.4 mg of PEDOT-RGO, 0.8 mg of conductive carbon, 300 µL of NMP, and 17.5 µL of Nafion was mixed in a mortar and ground with a pestle for a duration of 4 minutes.

(3) Then, the mixture was drop coated to the surface of the sliced graphite sheet and subjected to a drying process for a duration of 12 hours at a temperature of around 90 degrees Celsius.

(4) The part where the active material is coated was then pressed at a pressure of 0.5 tons for a duration of 15 seconds with a pellet press.

(5) The completed electrode was subsequently encased in tape, leaving only the coated section and the area for the wire connection exposed. It was then ready for the characterization.

Picture 2 shows the prepared PEDOT-RGO electrode.

Picture 2. PEDOT-RGO loaded electrode.

2.5 Characterization of PEDOT-RGO nanocomposite

The X-ray powder diffraction (XRD), Raman spectroscopy, and scanning electron microscope (SEM) were used to analyze and determine the composition and structure of the synthesized PEDOT-RGO in this work. And the electrochemical performance of the PEDOT-RGO supercapacitor was then evaluated using an electrochemical workstation.

2.5.1 XRD

XRD is an effective and non-destructive analytical method that provides accurate information on the crystallographic arrangement, phase composition, and physical properties of a material. The mechanism is founded on the idea that when a stream of X-rays interacts with a crystalline specimen, the X-rays undergo diffraction or scattering in a specific pattern. X-rays are a kind of electromagnetic radiation characterized by shorter wavelengths. They are generated when energetic charged particles undergo a reduction in energy. In XRD, the X-rays produced are focused and targeted at a sample material. The entering X-rays interact with the material, resulting in the creation of a diffracted ray. This ray is subsequently detected, examined, and measured. Then, the pattern of diffraction is generated by graphing the intensity of the scattered rays that are diffracted at different angles by a substance. X-ray diffractometers typically comprise an X-ray emitter, a sample holder, and a detector. The X-ray source generates a beam of X-rays that has a single wavelength and heads towards the sample. The detector collects the diffracted X-rays and measures their intensity and angle of diffraction. The distinct chemistry and atomic structure of the sample material result in a distinct diffraction pattern for each phase. By analyzing these resulting diffraction patterns, detailed information about the sample can be obtained, which is quite beneficial for identifying the sample.[32-34]

In this experiment, the formation of synthesized PEDOT-RGO nanocomposites was checked by XRD. Picture 3 exhibits the X-ray diffractometer utilized in the experiment. During the XRD test, the sample is evenly coated onto a glass slide, with copper serving as the substrate due to its favorable thermal conductivity, chemical stability, and minimal creation of background signals in XRD tests. The samples were analyzed using a Cu Kα source in "slow scan" mode.

Picture 3. Powder X-ray diffractometer.

2.5.2 Raman spectroscopy

RRaman spectroscopy is a highly effective and non-intrusive analytical technique offering comprehensive insights into the crystallinity, chemical structure, phase and polymorphy, and molecular composition of a material. This technique is based on the concept that the sample is subjected to monochromatic light, and the photons emitted by the laser interact with the molecules of the sample and scatter in a way that does not conserve energy. The dispersed light comprises wavelengths that are either unaltered (Rayleigh scattering) or altered (Raman scattering). Through the analysis of the Raman scattered light, it is possible to derive a distinctive representation of the chemical composition of the sample. The Raman spectrum exhibits a sequence of peaks that indicate the strength and vibrational patterns of the molecules present in the sample. Each peak corresponds to a certain vibration of a chemical bond, allowing for the analysis of molecular bonds, functional groups, crystal structures, and other material features.[35]

A Raman spectrometer typically comprises a laser light source, a monochromator, and a detector. The laser beam is focused on the sample during the measurement, and the dispersed light is then gathered and evaluated. Raman spectra are obtained by measuring the intensity and frequency of the scattered light, and they serve as a unique chemical signature for a certain molecule or substance, allowing for the rapid identification of the material and differentiation from others.

In this experiment, the functionality of PEDOT-RGO nanocomposites was identified by Raman spectroscopy. Picture 4 displays the Raman spectrometer utilized in the experiment. During the characterization process, PEDOT-RGO was first ground into a fine powder using a mortar and pestle to ensure that it obtained a uniform particle size distribution for Raman analysis. Subsequently, the sample is placed onto a glass slide and subjected to analysis using a Raman spectrometer equipped with a 532 nm laser operating at 5% power.

Picture 4. Raman spectrometer.

2.5.3 SEM

Scanning electron microscope (SEM) is a highly advanced and precise device that is utilized for investigating the surface morphology and composition of different materials with exceptional resolution. The technique relies on the utilization of a concentrated stream of electrons to examine the surface of the sample. The interaction between the electrons in the stream and the sample produces diverse signals, which can be gathered and analyzed to provide detailed images with high resolution. Subsequently, the obtained photographs can provide details on the topography and composition of the surface. In a usual scanning electron microscope (SEM) configuration, the electron beam is produced by a high-voltage electron source, such as a tungsten filament or a field-emission cathode and directed towards the sample by a sequence of electromagnetic lenses. In order to prevent electron scattering and absorption by other molecules in air, the sample is put in a vacuum chamber. During the scanning process, when the electron beam scans across the surface of the sample, there are interactions between the electrons in the beam and the atoms in the sample. These interactions cause the emission of different signals.[36]

SEM offers many measurement modes, such as secondary electron imaging, backscattered electron imaging, and transmission electron imaging. The main signal obtained in scanning electron microscopy (SEM) is secondary electrons (SE), which are low-energy electrons released from the surface of the sample due to the excitation of atoms by the incident electron beam. SE imaging offers precise and comprehensive information on the topography of surfaces, enabling the observation of surface characteristics, textures, and structures at the nanoscale. In addition, backscattered electrons (BSE) are electrons with greater energy that are dispersed in a backward direction from the surface of the sample as a result of interactions with the atomic nuclei. BSE imaging offers compositional contrast, where areas with greater atomic numbers exhibit increased brightness in the image.[36,37]

In this experiment, the morphology and structure of the prepared PEDOT-RGO nanocomposites were analyzed through a scanning electron microscope. Picture 5 shows the scanning electron microscope that has been used for the measurement. In the SEM sample preparation process, PEDOT-RGO was first dissolved in ethanol

utilizing sonication, a silicon wafer was used as a conductive substrate here. Then, the mixture was applied onto the substrate using a drop-coating technique and then dried in an oven. After that, the sample was ready for the measurement.

Picture 5. Scanning electron microscope.

2.5.4 Electrochemical workstation

The electrochemical workstation is a versatile scientific device utilized for the examination and analysis of diverse electrochemical processes within the area of electrochemistry. Electrochemical parameters, such as potentials and currents, can be easily controlled and detected using the electrochemical workstation. Electrodes are employed at the workstation to transmit and receive electrical signals. An electrochemical workstation typically comprises a working electrode, a counter electrode, and a reference electrode. The working electrode, as the main sensor, is

the place where most of the electrochemical reactions occur. The platinum electrode is commonly employed as the counter electrode owing to its exceptional conductivity. By utilizing the working electrode, a circuit can be established to provide a consistent flow of electric current. The standard reference electrode provides a dependable potential reference for measuring the continually changing potential of the working electrode.[38,39]

Picture 6 illustrates the electrochemical workstation that has been used for the measurement, which generally consists of two main components: potentiostat and galvanostat. The potentiostat works as the main control unit of the workstation, offering accurate regulation of the voltage provided to the working electrode and the current passing through the electrochemical cell. Potentiostat can be employed in various applications, such as studying redox reactions, corrosion, electroplating, and other processes that require a constant potential. It is also used in techniques like cyclic voltammetry, where the potential is swept across a range of values. Additionally, potentiostat is useful for investigating electrochemical behavior, kinetics, and the properties of electrode surfaces. Some electrochemical workstations have a galvanostat function, which enables accurate regulation of the current delivered to the electrochemical cell, in addition to voltage control. The galvanostat is commonly utilized in various applications, such as the study of electrolysis, electrodeposition, or any process that necessitates the maintenance of a constant current. It is also employed in experiments involving fuel cells, batteries, or other electrochemical cells that require a specific current input. Additionally, it is utilized in techniques like electrochemical impedance spectroscopy or other methods that analyze the electrical response of a system.[40]

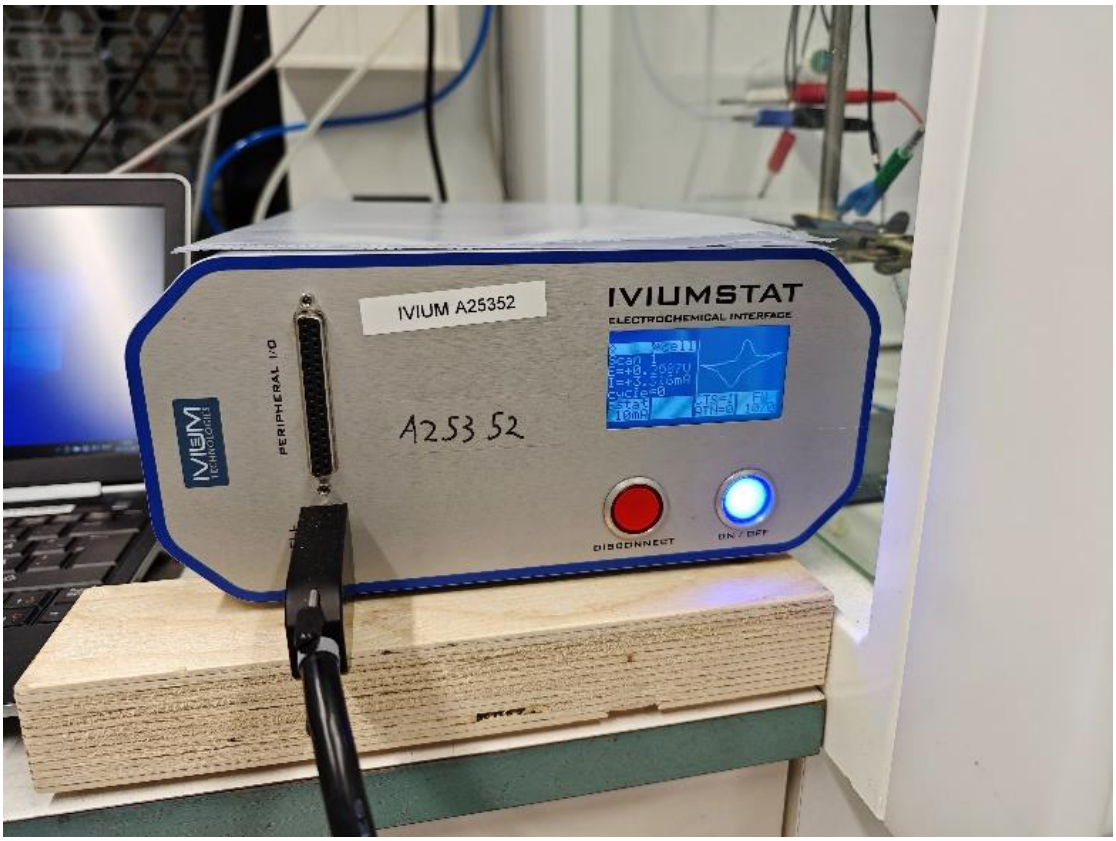

Picture 6. Electrochemical workstation.

In this experiment, the overall electrochemical performance of graphite sheet electrode, PEDOT electrode, and PEDOT-RGO electrode under the electrolyte of 1M sulfuric acid was evaluated by the electrochemical workstation, in which the cyclic voltammetry (CV), galvanic charging discharging (GCD), and electrochemical impedance spectroscopy (EIS) tests were carried out respectively. The tested electrode active materials were assembled into a symmetrical two-electrode cell setup under 1M H_2SO_4 electrolyte solution for electrochemical performance measurements, as it can be seen in Picture 7.

The CV measurements are conducted using various scan rates ranging from 5 to 500 mV/s (5 mV/s, 10 mV/s, 20 mV/s, 30 mV/s, 50 mV/s, 70 mV/s, 100 mV/s, 150 mV/s, 200 mV/s, 300 mV/s, 400 mV/s, and 500mV/s). The potential window for these measurements is set between 0V and 1V. The GCD measurements are performed at various current densities, ranging from 0.25 to 25 A/g, specifically at 0.25 A/g, 0.5 A/g, 1 A/g, 2 A/g, 3 A/g, 4 A/g, 5 A/g, 7 A/g, 10 A/g, 15 A/g, 20 A/g, and 25 A/g, in which these measurements are performed within a potential range of 0 to 1 V. The EIS

measurements were carried out using an amplitude of 0.02 V over a frequency range spanning from 1 MHz to 0.01 Hz.

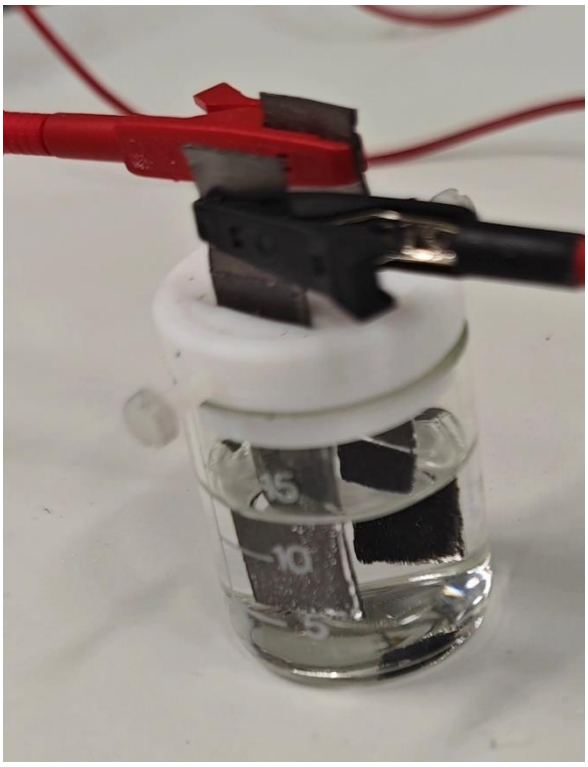

Picture 7. Assembled symmetric 2-electrode cell setup for electrochemical testing.

3 Results

3.1 Identification of PEDOT-RGO nanocomposites

The successful synthesis of PEDOT-RGO nanocomposite can be verified by XRD and Raman spectroscopy. Figure 16a presents the XRD spectra of PEDOT-RGO nanocomposite and GO. From which the XRD peaks for PEDOT are observed at 2θ = 6.8°, 12.9°, and 26.4°, which are respectively caused by the stacking of molecule ring in between chains along the orthorhombic a-axis, the reflection of the (100) plane in the (200) plane, and the intermolecular spacing of the PEDOT backbone or the (020) reflection. The sharp peak seen at 2θ = 6.8° is a distinctive feature of PEDOT, suggesting their exceptional crystallization and ordered structure.[41,42] From these characteristic peaks, the presence of PEDOT in PEDOT-RGO nanocomposites can be confirmed. The sharp XRD peak (001) of GO (at 2θ = 11.7°) shifted to the peak (002) with a higher 2θ value (2θ = 26.4°) after reduction in the nanocomposite, suggesting the reduction of GO to RGO.

Figure 16b exhibits the Raman spectra of the PEDOT-RGO nanocomposite with GO. The Raman spectra of the PEDOT-RGO nanocomposite showed distinctive peaks at 1431 cm^{-1} and 1508 cm^{-1}, which correspond to the symmetric stretching of $C_\alpha=C_\beta$ (-O) and the stretching of $C_\alpha=C_\beta$ in PEDOT, respectively.[43,44] The presence of these characteristic peaks can also provide evidence for the formation of PEDOT in the PEDOT-RGO nanocomposite. The D band at 1335 cm^{-1} and G band at 1577 cm^{-1} were appeared in the Raman spectra of GO, indicating the sp^2 and sp^3 hybridized carbon networks in graphene oxide. After the reduction process, the G band exhibited an increase in comparison to GO, indicating a reduction in functional groups and the restoration of π-conjugations as a result of the enhanced sp^2 carbon networks. In the Raman spectrum of PEDOT-RGO, the D band, and G band in GO were broadened, and the intensity ratio of the D band and G band (I_D/I_G) was decreased, suggesting the presence of RGO in PEDOT-RGO nanocomposite.[12]

The SEM image in Figure 16c shows PEDOT-RGO nanocomposite at a magnification of 5,000x. From which it can be seen that the thin sheets of RGO and PEDOT probably formed a porous structure by self-assembly. The existence of a porous structure can

act as a reservoir for ion buffering and enhance the transportation of ions along channels, hence promoting electrochemical kinetics.[12]

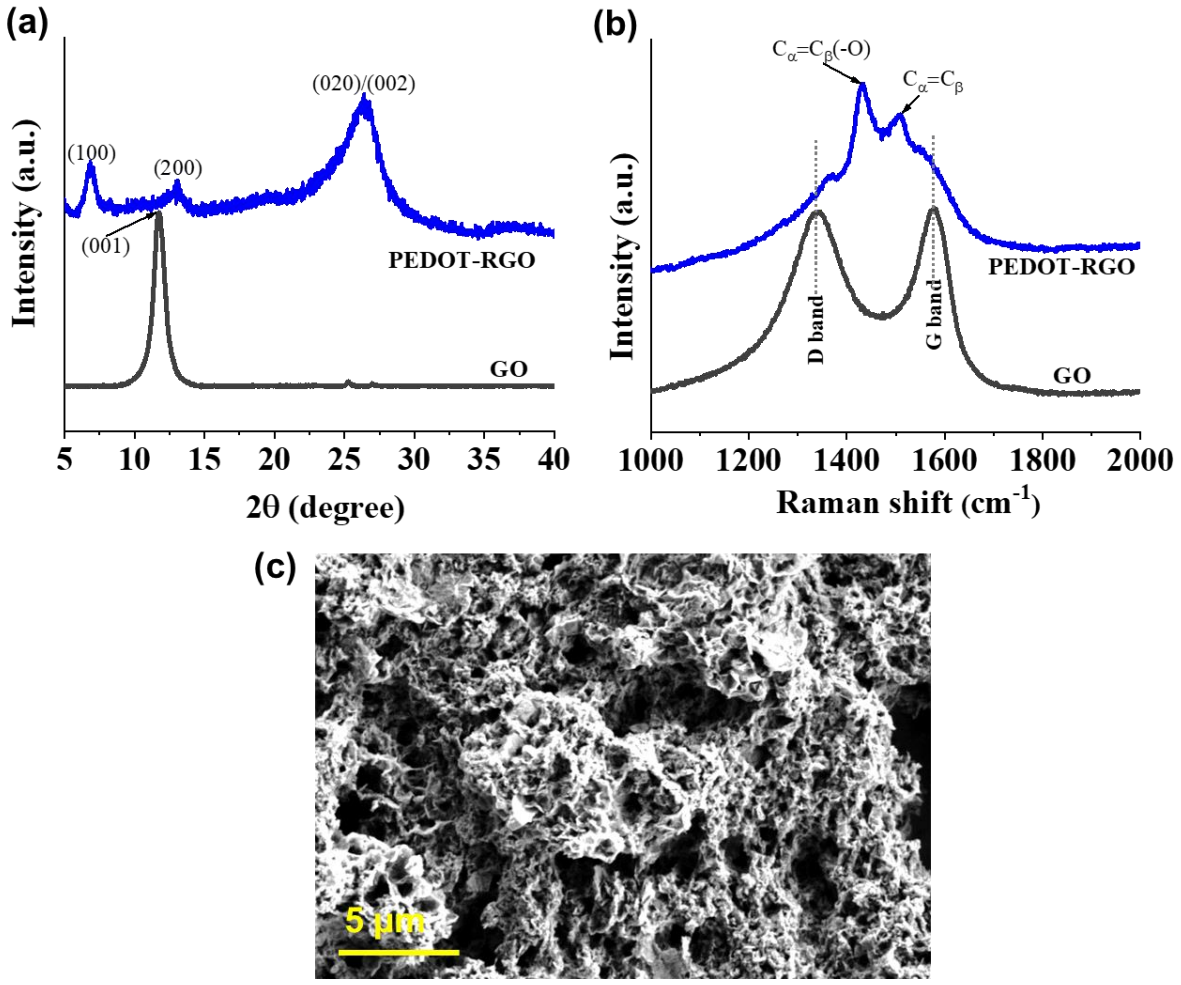

Figure 16. Characterization of PEDOT-RGO nanocomposites. (a) XRD spectrums of PEDOT-RGO and GO. (b) Raman spectrums of PEDOT-RGO and GO. (c) SEM image of the PEDOT-RGO at 5000x.

3.2 Electrochemical characterization of PEDOT-RGO supercapacitors

The CV curve of the PEDOT-RGO supercapacitor (Figure 17a) under 1 M sulfuric acid exhibits a shape very close to the rectangle, which suggests that the formation of the EDL at the interface of electrodes and the electrolyte, and it also indicates that the prepared PEDOT-RGO supercapacitor has good electrochemical reaction reversibility and fast electron transfer ability. Furthermore, through comparative analysis with the CV curve of the graphite sheet substrate, it can be seen that the capacitance of the

PEDOT-RGO supercapacitor mainly comes from the electrode active material itself and has little to do with the conductive graphite sheet substrate. Upon analyzing the CV curve of PEDOT, it can be seen that the doping of RGO as a filler into PEDOT improves the overall electrochemical performance of the supercapacitor. The triangular shape of the GCD plots of the PEDOT-RGO supercapacitor (Figure 17b) also suggests that the capacitance is mostly caused by EDL and high-charge mobility at the PEDOT-RGO electrode interface.

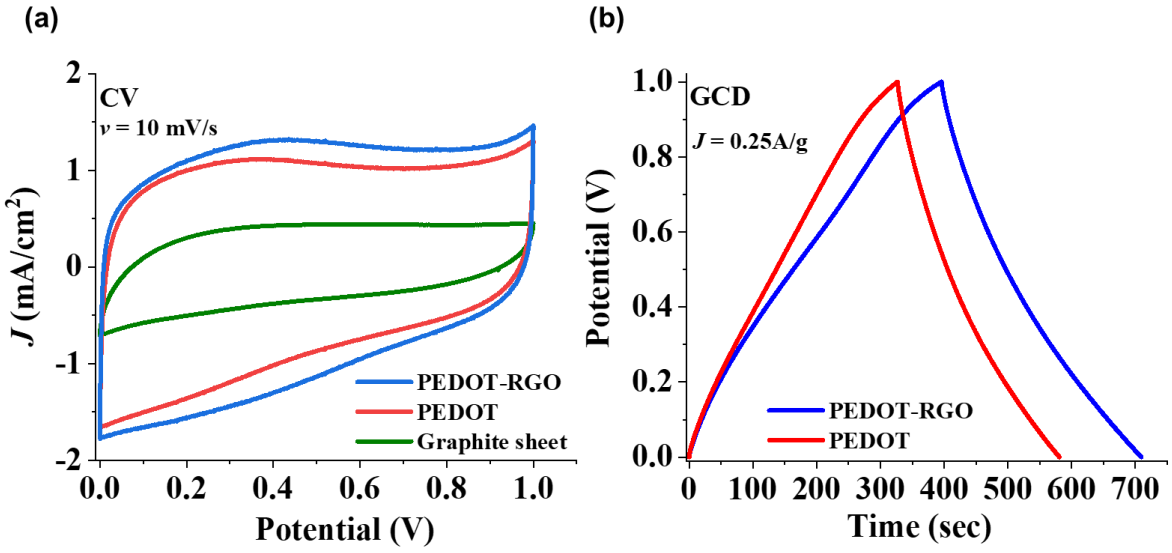

Figure 17. (a) CV plots of graphite sheet, PEDOT, and PEDOT-RGO supercapacitor in 1M sulfuric acid electrolyte at the scan rate of 10 mV/s. (b) GCD plots of PEDOT and PEDOT-RGO supercapacitor in 1M H_2SO_4 electrolyte at the current density of 0.25 A/g.

From electrochemical impedance spectroscopy (EIS), the overall resistance, as well as electrolyte ion transport in the electrode active material, can be analyzed. Figure 18a shows the Nyquist plots of PEDOT and PEDOT-RGO supercapacitor under 1 M sulfuric acid. From which it can be seen that the Nyquist plot of the PEDOT-RGO supercapacitor is almost vertical, and the zoomed-in area at high frequency displays a very small semicircle, suggesting an ideal capacitive behavior-- that is, very low charge-transfer resistance with high electrolyte diffusion within the PEDOT-RGO electrode. The equivalent series resistance (ESR), which is represented by the Nyquist plot's point of intersection with the real (Z) axis, was determined to be around 2.0 Ω for both the PEDOT and PEDOT-RGO supercapacitor under 1 M sulfuric acid. Figure 18b presents the Bode phase plot of the PEDOT-RGO supercapacitor from which the time

constant can be calculated according to formula 1, which was 1.94 seconds at a 45°phase angle.

$$\tau_0 = \frac{1}{f_0} \quad (1)$$

in which t_0 is the time constant, f_0 is the frequency at the phase angle of −45°.

Supercapacitors with lower time constants exhibit faster response to voltage fluctuations, making them more suited for high-frequency applications. The time constant of the PEDOT supercapacitor under the same condition was determined to be 2.07 seconds at a 45°phase angle. The improvement in the performance of the PEDOT-RGO supercapacitor can also be demonstrated by the change in the time constant resulting from the doping of RGO into PEDOT.

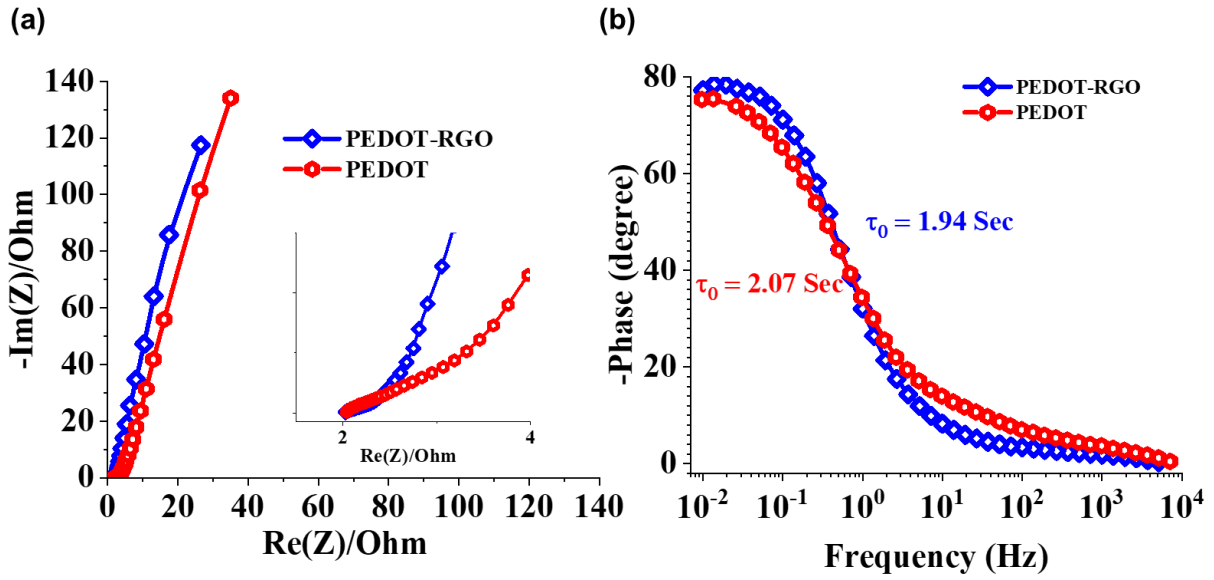

Figure 18. (a) Nyquist plots of PEDOT and PEDOT-RGO supercapacitor in 1M sulfuric acid electrolyte. (b) Bode phase plots of PEDOT and PEDOT-RGO supercapacitor in 1M sulfuric acid electrolyte.

Figure 19a displays the CV curves of PEDOT-RGO across a variety of scan rates, ranging from 5 to 500 mV/s. The presence of partial rectangular-shaped CV curves at both low and high scan rates indicates that ions can easily flow through the channels in the material. When comparing with the CV diagram of the PEDOT supercapacitor (Figure 19b), it can be observed that the comprehensive

electrochemical performance of the PEDOT-RGO supercapacitor is closer to the ideal supercapacitor.

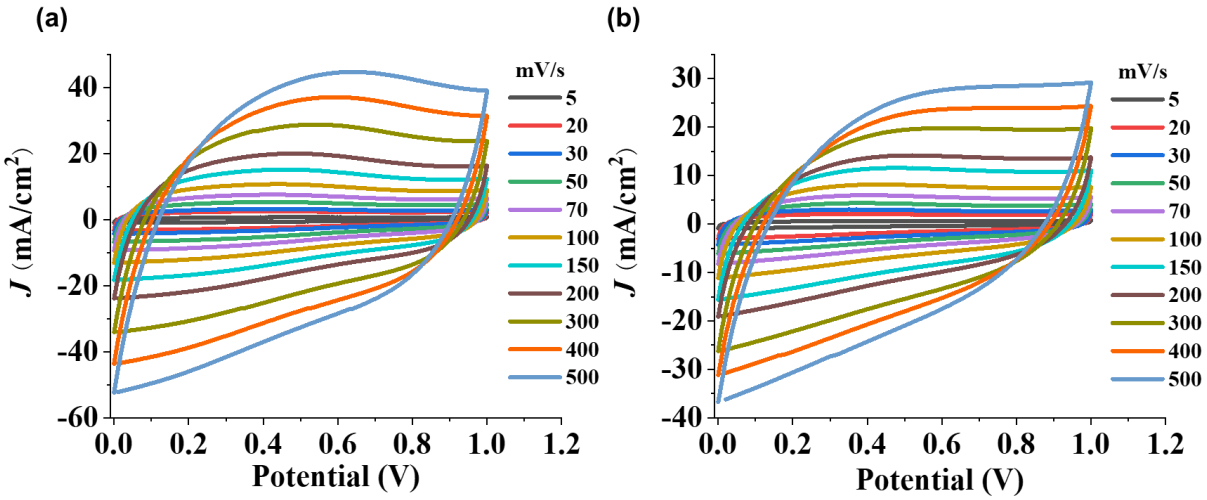

Figure 19. (a) CV plots of PEDOT-RGO supercapacitor in 1M H_2SO_4 electrolyte. (b) CV plots of PEDOT supercapacitor in 1M sulfuric acid electrolyte.

Figure 20 shows the GCD plots of PEDOT and PEDOT-RGO supercapacitors across a variety of current densities, ranging from 0.5 to 25 A/g under 1M H_2SO_4 electrolyte. These GCD plots can provide further evidence supporting the results obtained from the CV diagram.

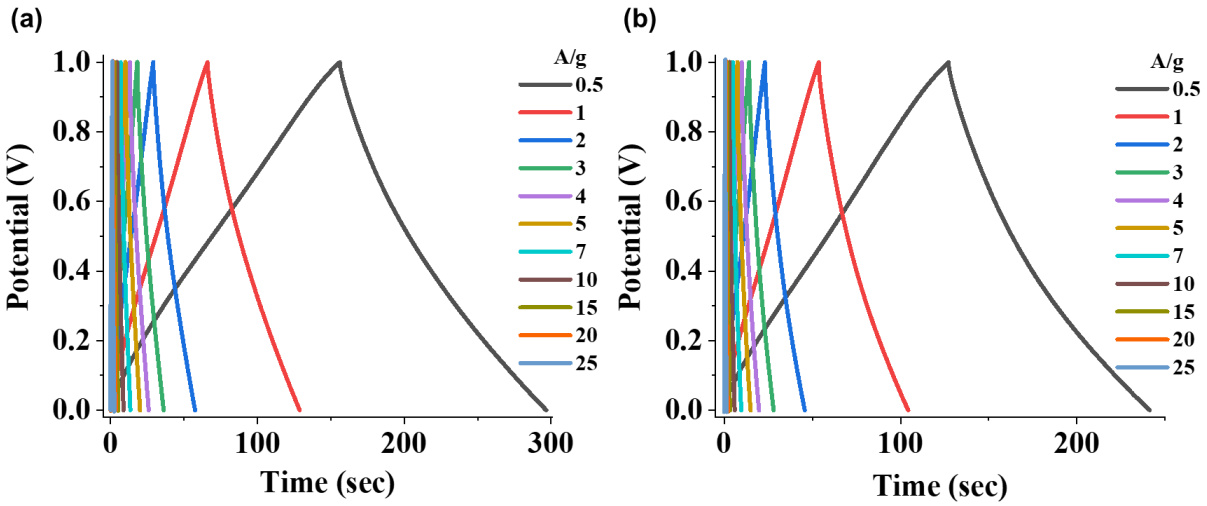

Figure 20. (a) GCD plots of PEDOT-RGO supercapacitor in 1M H_2SO_4 electrolyte. (b) GCD plots of PEDOT supercapacitor in 1M H_2SO_4 electrolyte.

The values of the specific capacitance collected from the GCD plots are displayed as a curve versus current density (J), as shown in Figure 21a. The capacitance of PEDOT and PEDOT-RGO supercapacitor under 1 M sulfuric acid can be calculated according to the formula 2, which were 128 F/g and 158 F/g respectively at a current density of 0.25 A/g. From Figure 21a, it can be proved that the capacitance value of the PEDOT-RGO supercapacitor was increased compared with the PEDOT supercapacitor after the doping of RGO.

$$C = \frac{I_{discharge}}{\frac{dV}{dt}}$$

$$C_G = 2 * \frac{C}{M} \quad (2)$$

in which, $I_{discharge}$ is the discharge current in mA, $\frac{dV}{dt}$ is the discharge curve's slope exclude the voltage (IR) drop in V/s, C_G is the gravimetric capacitance of the active material in an electrode in F/g, M is the mass of each electrode in grams (g).

Figure 21b displays the Ragone plots of the PEDOT and PEDOT-RGO supercapacitors. From which, the energy and power densities of these two supercapacitors under 1 M sulfuric acid can be calculated based on the formula 3. The maximum E_d and P_d values of the PEDOT supercapacitor are 4.4 Wh/kg and 4304 W/kg, respectively. The PEDOT-RGO supercapacitor has a maximum energy density of 5.4 Wh/kg and a maximum power density of 4655 W/kg. Through Figure 21b, it can be demonstrated that the energy and power densities of the PEDOT supercapacitor increased after incorporating reduced graphene oxide.

$$E_{d,G} = \frac{1}{8} C_G \times V^2 \times \frac{1000}{3600}$$

$$P_{d,G} = \frac{E_{d,G}}{t_{discharge}} \times 3600 \quad (3)$$

in which, $E_{d,G}$ is the gravimetric energy density in Wh/kg, V is the potential window ($V - V_{IR}$) in volts, $P_{d,G}$ is the gravimetric power density in W/kg, $t_{discharge}$ is the discharge time exclude the voltage (IR) drop in seconds (s).

Considering the significant energy consumption, it is necessary for supercapacitors to undergo numerous charge-discharge cycles. Therefore, the long-term cycling stability of the active material is of utmost importance. To assess the endurance of the PEDOT-RGO material, 10,000 continuous galvanic charge-discharge cycles were conducted at a current density of 10 A/g. The stability test showed more than 80% capacitance retention and 100% coulombic efficiency after 10,000 continuous GCD cycles, as it can be seen in Figure 21c.

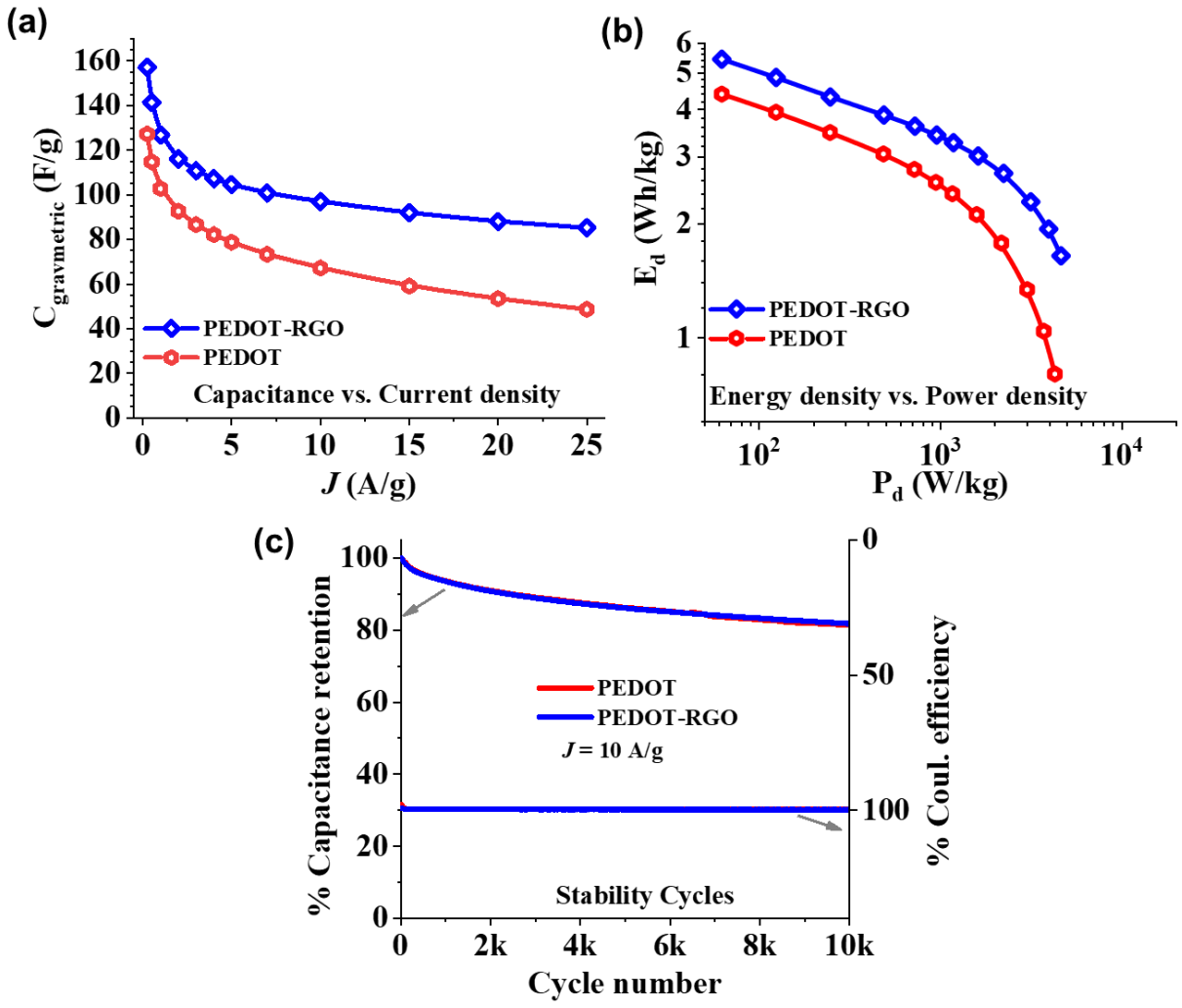

Figure 21. Electrochemical performance of PEDOT and PEDOT-RGO supercapacitor. (a) Plots of current density versus specific capacitance under the electrolyte of 1M H_2SO_4. (b) Ragone plots of PEDOT and PEDOT-RGO supercapacitor under the electrolyte of 1M H_2SO_4. (c) Stability cycles of PEDOT and PEDOT-RGO supercapacitor at the current density of 10 A/g.

4 Conclusion and discussion

In this thesis work, PEDOT-RGO nanocomposites with a porous structure were successfully prepared via an in-situ oxidation-reduction method, in which the Fe(III)PTS was used as the oxidation agent during the synthesis process. The prepared PEDOT-RGO nanocomposites were then checked through a series of characterization techniques, such as powder X-ray diffraction, Raman spectroscopy, and scanning electron microscope. The supercapacitors of the PEDOT and the synthesized PEDOT-RGO nanocomposites were successfully manufactured and evaluated within a symmetric 2-electrode setup and under a 1M H_2SO_4 electrolyte with the support of an electrochemical workstation. The results of the experiment suggest that the PEDOT-RGO supercapacitor achieves a maximum specific capacitance of 158 F/g at a current density of 0.25 A/g, which is 30 F/g more than that of the PEDOT supercapacitor. Besides, compared with the PEDOT supercapacitor, the PEDOT-RGO supercapacitor exhibited higher maximum values for energy density and power density, with about 1 Wh/kg and 351 W/kg increase, respectively. In addition, the PEDOT-RGO supercapacitor retained more than 80% of its capacitance and 100% coulombic efficiency after 10,000 continuous GCD cycles. Due to the restricted usage duration of the testing equipment, only 10,000 GCD cycles were conducted here. Although it could be challenging to distinguish the enhanced stability of PEDOT-RGO compared to PEDOT after 10,000 GCD cycles based on the figure, it can become more apparent with more charging and discharging cycles experienced by the supercapacitor. All these results can indicate that the overall supercapacitive performance of PEDOT was improved after the incorporation of reduced graphene oxide.

Overall, synthesizing PEDOT-RGO utilizing Fe(III)PTS was straightforward and could possibly end in developing efficient and environmentally friendly PEDOT-RGO supercapacitors.

References

(1) Sinha, P.; Kar, K. K. J. H. o. n. s. m. I. P. Introduction to supercapacitors. 2020, 1-28.

(2) Asumadu-Sarkodie, S.; Owusu, P. A. J. C. E. Feasibility of biomass heating system in Middle East Technical University, Northern Cyprus Campus. 2016, 3 (1), 1134304.

(3) Fan, E.; Li, L.; Wang, Z.; Lin, J.; Huang, Y.; Yao, Y.; Chen, R.; Wu, F. J. C. r. Sustainable recycling technology for Li-ion batteries and beyond: challenges and future prospects. 2020, 120 (14), 7020-7063.

(4) González, A.; Goikolea, E.; Barrena, J. A.; Mysyk, R. J. R.; reviews, s. e. Review on supercapacitors: Technologies and materials. 2016, 58, 1189-1206.

(5) Chakraborty, S.; Mary, N. J. J. o. T. E. S. An overview on supercapacitors and its applications. 2022, 169 (2), 020552.

(6) Sharma, K.; Arora, A.; Tripathi, S. K. J. J. o. E. S. Review of supercapacitors: Materials and devices. 2019, 21, 801-825.

(7) Kumar, N.; Kim, S.; Lee, S.; Park, S. Recent advanced supercapacitor: a review of storage mechanisms, electrode materials, modification, and perspectives. Nanomaterials, 2022; 12 (20): 3708. s Note: MDPI stays neutral with regard to jurisdictional claims in published …: 2022.

(8) Meng, C.; Gall, O. Z.; Irazoqui, P. P. J. B. m. A flexible super-capacitive solid-state power supply for miniature implantable medical devices. 2013, 15, 973-983.

(9) Häggström, F.; Delsing, J. J. E. h.; systems. Iot energy storage-a forecast. 2018, 5 (3-4), 43-51.

(10) Halper, M. S.; Ellenbogen, J. C. J. T. M. C., McLean, Virginia, USA. Supercapacitors: A brief overview. 2006, 1.

(11) Pandolfo, A. G.; Hollenkamp, A. F. J. J. o. p. s. Carbon properties and their role in supercapacitors. 2006, 157 (1), 11-27.

(12) Jha, P. K.; Gupta, K.; Debnath, A. K.; Rana, S.; Sharma, R.; Ballav, N. J. C. 3D mesoporous reduced graphene oxide with remarkable supercapacitive performance. 2019, 148, 354-360.

(13) Jalal, N. I.; Ibrahim, R. I.; Oudah, M. K. A review on Supercapacitors: Types and components. In Journal of Physics: Conference Series, 2021; IOP Publishing: Vol. 1973, p 012015.

(14) Şahin, M. E.; Blaabjerg, F.; Sangwongwanich, A. J. E. A comprehensive review on supercapacitor applications and developments. 2022, 15 (3), 674.
(15) Umoren, S. A.; Solomon, M. M.; Saji, V. S. Polymeric materials in corrosion inhibition: fundamentals and applications; Elsevier, 2022.
(16) Shahabuddin, S.; Mazlan, N. A.; Baharin, S. N. A.; Sambasevam, K. P. J. A. i. h. c. p. t. Introduction to conducting polymers. 2021, 1-18.
(17) Del Valle, M.; Gacitúa, M.; Hernández, F.; Luengo, M.; Hernández, L. J. P. Nanostructured conducting polymers and their applications in energy storage devices. 2023, 15 (6), 1450.
(18) Das, T. K.; Prusty, S. J. P.-p. t.; engineering. Review on conducting polymers and their applications. 2012, 51 (14), 1487-1500.
(19) Namsheer, K.; Rout, C. S. J. R. a. Conducting polymers: a comprehensive review on recent advances in synthesis, properties and applications. 2021, 11 (10), 5659-5697.
(20) Chamoli, P.; Banerjee, S.; Raina, K.; Kar, K. K. J. H. o. N. S. M. I. C. Characteristics of graphene/reduced graphene oxide. 2020, 155-177.
(21) Allen, M. J.; Tung, V. C.; Kaner, R. B. J. C. r. Honeycomb carbon: a review of graphene. 2010, 110 (1), 132-145.
(22) Hansora, D.; Shimpi, N.; Mishra, S. J. J. Graphite to graphene via graphene oxide: an overview on synthesis, properties, and applications. 2015, 67, 2855-2868.
(23) Urade, A. R.; Lahiri, I.; Suresh, K. J. J. Graphene properties, synthesis and applications: a review. 2023, 75 (3), 614-630.
(24) Hernaez, M.; Zamarreño, C. R.; Melendi-Espina, S.; Bird, L. R.; Mayes, A. G.; Arregui, F. J. J. S. Optical fibre sensors using graphene-based materials: A review. 2017, 17 (1), 155.
(25) Bhuyan, M. S. A.; Uddin, M. N.; Islam, M. M.; Bipasha, F. A.; Hossain, S. S. J. I. N. L. Synthesis of graphene. 2016, 6, 65-83.
(26) Groenendaal, L.; Zotti, G.; Aubert, P. H.; Waybright, S. M.; Reynolds, J. R. J. A. M. Electrochemistry of poly (3, 4‐alkylenedioxythiophene) derivatives. 2003, 15 (11), 855-879.
(27) Rahimzadeh, Z.; Naghib, S. M.; Zare, Y.; Rhee, K. Y. J. J. o. m. s. An overview on the synthesis and recent applications of conducting poly (3, 4-

ethylenedioxythiophene)(PEDOT) in industry and biomedicine. 2020, 55, 7575-7611.

(28) Groenendaal, L.; Jonas, F.; Freitag, D.; Pielartzik, H.; Reynolds, J. R. J. A. m. Poly (3, 4‐ethylenedioxythiophene) and its derivatives: past, present, and future. 2000, 12 (7), 481-494.

(29) Maity, S.; Datta, S.; Mishra, M.; Banerjee, S.; Das, S.; Chatterjee, K. J. P. f. A. T. Poly (3, 4 ethylenedioxythiophene)‐tosylate—Its synthesis, properties and various applications. 2021, 32 (4), 1409-1427.

(30) Tarcan, R.; Todor-Boer, O.; Petrovai, I.; Leordean, C.; Astilean, S.; Botiz, I. J. J. o. M. C. C. Reduced graphene oxide today. 2020, 8 (4), 1198-1224.

(31) Ray, S. Applications of graphene and graphene-oxide based nanomaterials; William Andrew, 2015.

(32) Inan, T. Thermoplastic-based nanoblends: Preparation and characterizations. In Recent developments in polymer macro, micro and nano blends, Elsevier, 2017; pp 17-56.

(33) Raja, P. B.; Munusamy, K. R.; Perumal, V.; Ibrahim, M. N. M. Characterization of nanomaterial used in nanobioremediation. In Nano-bioremediation: fundamentals and applications, Elsevier, 2022; pp 57-83.

(34) Das, R.; Ali, E.; Abd Hamid, S. B. J. R. o. A. M. S. CURRENT APPLICATIONS OF X-RAY POWDER DIFFRACTION-A REVIEW. 2014, 38 (2).

(35) Olubiyi, O. I.; Lu, F.-K.; Calligaris, D.; Jolesz, F. A.; Agar, N. Y. Advances in molecular imaging for surgery. In Image-guided neurosurgery, Elsevier, 2015; pp 407-439.

(36) Mohammed, A.; Abdullah, A. Scanning electron microscopy (SEM): A review. In Proceedings of the 2018 International Conference on Hydraulics and Pneumatics—HERVEX, Băile Govora, Romania, 2018; Vol. 2018, pp 7-9.

(37) Inkson, B. J. Scanning electron microscopy (SEM) and transmission electron microscopy (TEM) for materials characterization. In Materials characterization using nondestructive evaluation (NDE) methods, Elsevier, 2016; pp 17-43.

(38) Hiesgen, R.; Haiber, J. Measurement Methods| Structural Properties: Atomic Force Microscopy. 2009.

(39) Li, G. Nano-inspired biosensors for protein assay with clinical applications; Elsevier, 2018.

(40) Smith, J.; Hinson-Smith, V. Product review: The potentiostat: Electrochemistry's utility player. ACS Publications: 2002.

(41) Ni, D.; Chen, Y.; Song, H.; Liu, C.; Yang, X.; Cai, K. J. J. o. M. C. A. Free-standing and highly conductive PEDOT nanowire films for high-performance all-solid-state supercapacitors. 2019, 7 (3), 1323-1333.

(42) Zhang, L.; Jamal, R.; Zhao, Q.; Wang, M.; Abdiryim, T. J. N. r. l. Preparation of PEDOT/GO, PEDOT/MnO 2, and PEDOT/GO/MnO 2 nanocomposites and their application in catalytic degradation of methylene blue. 2015, 10, 1-9.

(43) Yewale, R.; Damlin, P.; Salomäki, M.; Kvarnström, C. J. M. T. C. Layer-by-layer approach to engineer and control conductivity of atmospheric pressure vapor phase polymerized PEDOT thin films. 2020, 25, 101398.

(44) Zhao, Q.; Jamal, R.; Zhang, L.; Wang, M.; Abdiryim, T. J. N. r. l. The structure and properties of PEDOT synthesized by template-free solution method. 2014, 9, 1-9.